https://doi.org/10.5194/egusphere-2026-2366
Preprint. Discussion started: 13 May 2026

C-CWatM v1.0: A high-resolution water resources and river routing model enabling direct linkage to state-of-the-art Earth-system and land-surface models

Peter Greve[1], Amelie U. Schmitt[1], Sina Jasmin Schreiber[1], Augustin Cledat[1,2], and Peter Burek[3]

[1]Climate Service Center Germany (GERICS), Helmholtz-Zentrum Hereon, Hamburg, Germany
[2]Laboratoire de Météorologie Dynamique/IPSL - Ecole Polytechnique/CNRS, Paris, France France
[3]Water Security Research Group, International Institute for Applied Systems Analysis (IIASA), Laxenburg, Austria

Correspondence: Peter Greve (peter.greve@hereon.de)

Abstract. River routing and human water management are often poorly represented in many Earth-system and land-surface models, not permitting consistent assessments of human-water-climate interactions. In this work, we introduce C-CWatM v1.0 (Climate-CWatM v1.0), a land-surface-driven version of the Community Water model (CWatM) that enables online and offline simulations of river routing, water resource availability, and management. The model operates on standard land-surface output and includes an OASIS3-MCT coupling interface, enabling efficient two-way coupling with Earth-system and land-surface models. In comparison to CWatM, all modules related to land-surface and snow processes have been removed to prevent conflicts with land-surface parameterisations implemented in the coupled models. C-CWatM also offers options for reducing-forcing requirements and simple on-the-fly bias correction using predefined quantile weights. We test C-CWatM in both online and offline settings and evaluate the model performance in offline mode using REMO output across a European domain. C-CWatM reproduces large-scale discharge patterns and hydrological gradients when using non-bias-corrected forcing data without calibration of model parameters. Calibration results in moderate improvements in model performance, while quantile-mapping-based bias correction of runoff significantly enhances model skill. A reduced-forcing version of the model enables rapid simulations based on available climate model output, as demonstrated using readily available EURO-CORDEX output. C-CWatM provides a novel and flexible hydrological and water resources modelling tool for representing river routing and water management in coupled modelling systems, enabling more integrated analyses of climate-water-human interactions.

1 Introduction

Water cycling through the various spheres of the Earth system is one of the fundamental organising principles of Earth system science, linking the energy and water balance, ecosystems, soils and climate. However, the natural water cycle is increasingly shaped by human activity, not only through anthropogenic climate change and land-use/land-cover change, but also through a growing, direct, and engineered redistribution of freshwater across the land surface. Large-scale human water management alters land surface processes, land-atmosphere interactions and terrestrial water storage via irrigation, damming and reservoirs, water transfers, desalination, and other interventions (Vörösmarty and Sahagian, 2000; Huang et al., 2015; Nazemi

https://doi.org/10.5194/egusphere-2026-2366
Preprint. Discussion started: 13 May 2026

and Wheater, 2015; McDermid et al., 2023; Tapiador and Navarro, 2024; Maina et al., 2025). Humans add an essential anthropogenic layer to the terrestrial water cycle. Human impact on freshwater systems is expected to further intensify due to population growth, rising food and energy demand, and increasing socio-economic needs (Holland et al., 2015; D'Odorico et al., 2018; Rodell et al., 2018; Yoon et al., 2021; Greve et al., 2023). In addition, changes in the water cycle and climate change are contributing to mounting water scarcity in many regions worldwide, which adds pressure on food security, energy production, and domestic and industrial water supply (Schewe et al., 2014; Mekonnen and Hoekstra, 2016; Greve et al., 2018; Huang et al., 2021; Rosa and Sangiorgio, 2025).

Water scarcity, changing water availability, and more frequent and intense hydroclimatic extremes amplify the need for large-scale water management to sustain yields, energy production, and municipal water supply. However, large-scale infrastructure and unsustainable withdrawals from surface and groundwater sources may degrade aquatic ecosystems, reduce environmental flows, and deplete groundwater resources (Elliott et al., 2014; Reid et al., 2019; Jia et al., 2020; Haase et al., 2023). In addition to hydrological impacts, water management alters various land-surface processes, potentially modifying land-atmosphere interactions and local-to-regional hydroclimatic conditions. Large-scale interventions such as irrigation, dams, and reservoirs significantly affect surface water and energy partitioning and terrestrial water storage (Zhou et al., 2020; Lv et al., 2021; Vanderkelen et al., 2021; Rappin et al., 2022; Lawston-Parker et al., 2023; Li et al., 2023). Irrigation, as the primary use of freshwater by humans (McDermid et al., 2023), has been shown to influence local and regional water cycles, affecting evaporation, hydroclimatic extremes (Thiery et al., 2020; Mishra et al., 2020; Li et al., 2022), and rainfall patterns (Alter et al., 2015; Yang et al., 2017; Song et al., 2024), especially downstream of irrigated areas (Greve et al., 2025; Zhang et al., 2025).

Despite the widespread impacts, significant gaps remain in our understanding of the interplay between (i) human water management at the land surface, (ii) local to basin-scale hydrology and water availability, and (iii) local to remote hydroclimatological and atmospheric responses. A significant reason for our lack of understanding is that many state-of-the-art earth system models misrepresent or omit critical processes, such as river routing, sectoral withdrawals, groundwater pumping, and dam/reservoir operations, thereby significantly limiting our ability to consistently quantify impacts across scales and disciplines. However, recent modelling advances enable more detailed assessments. An increasing number of climate and land surface models include various aspects of human water management, such as irrigation (e.g. Xu et al., 2019; Valmassoi et al., 2020; Zhou et al., 2020; Yao et al., 2022; Druel et al., 2022; Asmus et al., 2023; Arboleda-Obando et al., 2024; Decharme et al., 2025) and dams/reservoirs (Zhou et al., 2020; Vanderkelen et al., 2021), to enhance our understanding of altered land–atmosphere interactions. However, representations of human water use, such as irrigation withdrawals and reservoir operations, remain overly simplistic in ESMs. Efforts to improve the representation of water use in climate models are still limited. In the MIROC Earth System Model (MIROC ESM), human water withdrawals are integrated into the land surface component (Yokohata et al., 2020). The Community Earth System Model (CESM) incorporates water withdrawals using monthly input maps (Taranu et al., 2024). In the Earth System Model developed by the French National Centre for Meteorological Research, irrigation withdrawals can be sourced from groundwater and conceptual dams (Decharme et al., 2025). In parallel, global hydrological and water resources models include more and more sophisticated large-scale model representation of river flows, water storage, and the management and allocation of limited water resources across sectors (Hanasaki et al., 2018; Sutanudjaja et al.,

https://doi.org/10.5194/egusphere-2026-2366
Preprint. Discussion started: 13 May 2026

2018; Burek et al., 2020; Müller Schmied et al., 2021). These models are widely used to investigate the impacts on streamflow, groundwater reservoirs, and water availability.

However, despite significant advances in both large-scale hydrological and earth-system modelling, these efforts often remain disconnected. Hydrological models are implemented in offline mode (only driven by climate forcing data). In contrast, most climate and earth system models lack a dynamic representation of sectoral water withdrawals, sometimes enforce unlimited water use, and omit effective river routing, making it difficult to realistically constrain water use. In a movement towards a holistic representation of Earth system processes within more unified modelling systems, we identify a clear need for realistic, scalable representations of human water use and water management across land, hydrological, climate, and Earth system models. Implementing a fully coupled modelling system that builds on the state-of-the-art in global hydrology and Earth system modelling can close the gap between water management, hydrology, and land–atmosphere interactions, which is essential for sustainable and accessible assessments of future water availability, hydroclimatic extremes, and associated adaptation efforts.

In this study, we present the flexible water resources and river routing modelling tool Climate-CWatM (C-CWatM), which uses land-surface model output as input and includes a coupling interface for quick integration with existing climate and Earth system models. Our model is open source, modular, and implemented in Python, ensuring wide accessibility and easy extensibility. The model features river routing, a linear groundwater reservoir, sector-specific human water withdrawals, and dams and reservoirs, providing an innovative modelling approach to represent water management in upcoming coupled modelling frameworks consistently.

2 Model concept

Climate-CWatM (C-CWatM) is an integrated river-routing and water-resources model that uses land-surface variables as input. This design enables a direct linkage to state-of-the-art climate, Earth system, and land-surface modelling systems. Such models include a sophisticated representation of the land-surface and related processes but often lack river routing and water-management parameterisations. C-CWatM addresses this gap by providing estimates of water availability, human water demand across various sectors, and water abstraction from different sources building on the experience of nearly two decades of global hydrological and water-resources modelling. C-CWatM offers a new approach for simulating river routing and water management in offline mode, and in online mode when integrated with climate or Earth system models through a coupling interface.

C-CWatM is implemented as a simplified version of the Community Water Model (CWatM). The original development of CWatM (Burek et al., 2020) includes land-surface processes such as runoff generation, soil water dynamics, and evapotranspiration, which are also consistently represented within climate and Earth system models. To avoid duplicating land-surface processes in coupled modelling systems, the respective modules were removed, leaving a streamlined model focused on river routing and water management. See Sect. 3 for details about the remaining processes and their modifications.

Like CWatM, C-CWatM is a grid-based model available at two native spatial resolutions (5′ and 0.5°), and operates at a daily time step. Its hydrological processes, water-demand calculations, and data-handling routines are organised into separate

https://doi.org/10.5194/egusphere-2026-2366
Preprint. Discussion started: 13 May 2026

Figure 1. Schematic overview of forcing and processes in C-CWatM in comparison to traditional offline modelling approaches. C-CWatM includes a coupling interface and requires land surface input: runoff, soil moisture, drainage and open water evaporation (OWE). This figure is based on material from the CWatM GitHub repository (https://github.com/iiasa/CWatM, last access: 24.04.2026) modified and used under the GNU General Public License v3.0.

modules. This modular structure enables clear separation of tasks and efficient modification or extension of each component. Data reading and writing, as well as the coupling routine, are likewise implemented in dedicated modules.

C-CWatM builds on the overall structure of CWatM, but its modules have been adapted to use land-surface inputs and to enable the implementation of a coupling interface (Fig. 1). Variables that are computed internally in CWatM through its land-surface routines are instead provided as external forcing to C-CWatM. While CWatM requires atmospheric forcing, C-CWatM requires the following land surface input: runoff, (rootzone) soil moisture, evaporation from open water surfaces, and groundwater recharge (sometimes referred to as drainage in other models). Runoff, evaporation from open water surfaces and drainage are required in m/day. Soil moisture must be provided as the fraction of the available water in the soil relative to its water-holding capacity (relative saturation). Unit conversion factors can be included in a settings file, such that no prior data conversion is required. If information on open water evaporation is not available, C-CWatM offers the option to estimate potential evaporation over open water using temperature or net radiation input (Sect. 4.4).

The model is implemented primarily in Python, while computationally intensive river-routing routines are more efficiently integrated in C++ (see https://github.com/UWaRes/c-cwatm, last access: 24.04.2026). C-CWatM relies on a small set of Python packages (numpy, scipy, gdal, netCDF4, and pyOASIS for coupling). The flexibility of Python combined with the modular structure of C-CWatM enables quick modifications to the code, enhances accessibility for users and developers, and simplifies the integration of new functionalities. NetCDF serves as the main data format, with GeoTIFF also supported for input datasets. C-CWatM follows the CF Metadata Convention 1.6, providing the option to adjust metadata definitions following other conventions.

https://doi.org/10.5194/egusphere-2026-2366
Preprint. Discussion started: 13 May 2026

Coupling is implemented using the pyOASIS interface (Sect. 4.1), enabling two-way coupling between C-CWatM (in Python) and any model featuring an OASIS coupling interface, independent of the programming language. While OASIS is widely used in Earth system modelling, not all modelling systems include OASIS support. However, the modular implementation within C-CWatM serves as a blueprint for the integration of alternative coupling frameworks.

C-CWatM is ready to use and includes a settings file that features all configuration options. This approach increases accessibility for users with limited modelling experience or without prior familiarity with Python. C-CWatM comes with a GNU GENERAL PUBLIC LICENSE and is hosted on GitHub (https://github.com/UWaRes/c-cwatm/, last access: 24.04.2026) to enable easy access to the source code. Input data are similar to the input data used for CWatM and are freely available through CWatM repositories. C-CWatM comes with an extensive user handbook (C-CWatM user guide, 2026) summarising the model structure, the individual modules, installation procedure, model setup, data handling and configuration options in the settings file.

3 Overview of processes

Generally, all processes in C-CWatM are directly based on CWatM (Burek et al., 2020), with the following modifications: All hydrological processes related to soil, vegetation, snow, as well as evaporation and transpiration, are excluded in C-CWatM. Instead, the necessary variables are provided as external forcing. The following sections present an overview of the remaining processes and the required adjustments. A more detailed description of different model configurations, options and variables specified in the settings file is provided in the user guide (C-CWatM user guide, 2026).

3.1 River routing, reservoirs and lakes

The implementation of river routing and reservoirs and lakes in C-CWatM follows the same approach as in CWatM. River routing is based on the kinematic wave equations (Chow et al., 1998) and applied to a fixed channel network. The parameters of the equation are derived using Manning's equation, which requires information about channel width, depth, length, and gradient. Channel roughness, represented by Manning's coefficient, serves as a calibration parameter within the model.

Reservoirs and lakes are integrated into the channel network, distinguishing between global and local water bodies based on their size and catchment area. The categorization into global and local water bodies depends on the model resolution. Local reservoirs and lakes are situated within a single grid cell, and affect only local runoff processes and are not connected to the main river itself. In contrast, global reservoirs and lakes are located on the primary river channel of a grid cell and are connected to the entire upstream catchment..

The reservoir operation scheme is based on the LISFLOOD model (Burek et al., 2013). Reservoirs are managed within a defined normal operating range to maintain a consistent outflow, particularly to support hydropower generation. The outflow is calculated as a function of the reservoir's storage level and inflow conditions. Regulation is bounded by minimum and maximum thresholds to ensure ecological minimum flows and to prevent downstream flooding.

https://doi.org/10.5194/egusphere-2026-2366
Preprint. Discussion started: 13 May 2026

Lakes are simulated using a simplified flood retention approach, the modified Puls method (Chow et al., 1998; Burek et al., 2013). Changes in lake storage are calculated as the difference between inflow from upstream river channels and the combined effects of outflow and evaporation. The outflow is governed by lake water levels and outlet characteristics, with assumptions simplifying the geometry and flow dynamics. In the original CWatM implementation, lake evaporation is estimated using the potential evaporation rate over water surfaces. In C-CWatM, this has been simplified by incorporating open water evaporation as an external forcing field.

3.2 Groundwater

As in the CWatM model, groundwater storage and baseflow in C-CWatM are represented using a linear reservoir approach, following the methodology used in the LISFLOOD model (De Roo et al., 2000; Udias et al., 2016). This means that the outflow from the groundwater zone (baseflow) is proportional to the groundwater storage, with the recession coefficient determining the outflow rate. This recession coefficient serves as a calibration parameter within the model. Compared to CWatM, C-CWatM includes fewer groundwater processes. The reservoir is filled only by drainage from the lower soil zone and is depleted by baseflow and additional human groundwater abstraction for irrigation. In contrast, CWatM also accounts for preferential flow as a source term and capillary rise as a sink (Burek et al., 2020). Both are excluded in C-CWatM since these processes are often not considered in land surface and (regional) climate models.

3.3 Human water use

3.3.1 Irrigation water demand

Paddy irrigation for rice fields and irrigation for other crops are treated separately when calculating water withdrawal and consumption. As in CWatM, the default method for estimating water demand for non-paddy irrigation ($\mathrm{WD}_{\mathrm{irri}}$) is based on the difference between the target water amount and the available water in the root zone. The target water amount is defined as the difference between field capacity (FC) and wilting point (WP), scaled by an alpha-depletion factor (α), which can be specified in the settings file or implemented as a calibration parameter. The available water is calculated as the difference between the current soil water content in the root zone (SWC) and the wilting point. Thus, the irrigation water demand is given by:

$$\mathrm{WD}_{\mathrm{irri}} = \alpha(\mathrm{FC} - \mathrm{WP}) - (\mathrm{SWC} - \mathrm{WP}), \tag{1}$$

where SWC is derived by multiplying the root zone soil moisture (`rootzoneSM`, expressed in %) by the maximum soil water storage capacity. Maps for FC, WP and soil water storage capacity are loaded according to the settings file (and can be adapted to maps obtained from the driving land surface and climate model), while `rootzoneSM` is one of the required forcing fields in C-CWatM.

As in CWatM, the calculated irrigation water demand is constrained by the maximum infiltration capacity of the soil and a minimum irrigation limit (to avoid rounding issues). Irrigation is applied only during the growing season, which is determined using crop coefficient data (see Burek et al. (2020) and references therein for details). Water withdrawn for irrigation is typically

https://doi.org/10.5194/egusphere-2026-2366
Preprint. Discussion started: 13 May 2026

subject to losses during transport from the source to the field, as well as through return flows and evaporation occurring during the irrigation process. These losses are accounted for using an irrigation water use efficiency factor, which can either be specified as efficiency maps (e.g., based on country-level values) or set as a constant.

In the original implementation of CWatM, paddy irrigation is represented by maintaining a surface water depth of 50 mm, with water demand calculated as the difference between current and target water levels. To our knowledge, no land surface or (regional) climate model currently incorporates paddy irrigation in this manner. Consequently, the water level height - which would be needed as forcing data - cannot be provided. Therefore, we adopted a simplified approach to represent paddy irrigation in C-CWatM. This method follows the same principle as described before for non-paddy irrigation, with one key difference: the target soil water is always set to field capacity, implying an alpha-depleton factor of $\alpha = 1$.

3.3.2 Water demand from other human sources

Like in CWatM, the methods for calculating livestock, industrial, and domestic water demand are based on the approaches of Wada et al. (2011). Livestock water consumption is estimated based on the livestock densities in each grid cell. Each of the six livestock types considered has distinct drinking water requirements, which vary monthly as a function of air temperature.

Industrial water demand is calculated by multiplying a water use intensity index with a gridded dataset of industrial water demand for 2000 (based on Shiklomanov, 2000a). Water use intensity is derived from per capita values for gross domestic product (GDP), electricity production, energy consumption, and household consumption, capturing both economic and technological development. Similarly, domestic water demand is calculated by multiplying the same water use intensity index with the number of persons per grid cell and a country-specific per capita water withdrawal. Seasonal variability is considered by using air temperature as a proxy, with higher demand in warmer months. A large portion of the water withdrawn for both industrial and domestic purposes is returned to the river system after use. Consequently, the net water demand, representing actual consumption by industries and households, is adjusted based on return rates reported by Shiklomanov (2000b): industrial water use returns 90 %, and domestic water use returns 85 % to the system.

3.3.3 Water abstraction by source

Water demand for irrigiation, livestock, industry, and households can be fulfilled by surface water and groundwater resources. We adapt the approach for calculating water withdrawal from different sources from CWatM. By default, water is drawn in the following sequence: surface water is utilized first, starting with channels, followed by big lakes and reservoirs, and finally small lakes. If surface water alone cannot meet the demand, additional water is drawn from renewable groundwater. If local supply is insufficient, the model draws water from a buffer zone around lakes and reservoirs and then from a defined radius of neighboring grid cells for available surface and groundwater. If the demand is still not met, users can configure whether the remaining demand should persist as unmet demand or be fulfilled by non-renewable ground water, by setting the `limitAbstraction` parameter in the settings file.

In addition to human water demand, an environmental flow cap can be defined using external data. This cap represents the minimum flow required to sustain ecological functions in rivers, reservoirs, and lakes. The sequence in which water is drawn

https://doi.org/10.5194/egusphere-2026-2366
Preprint. Discussion started: 13 May 2026

from different sources can be customized by specifying source abstraction fractions for each sector. These fractions determine the proportion of water that should be extracted from rivers, lakes, and groundwater to meet the sector-specific demand.

4 Model enhancements and optional features

4.1 The OASIS3-MCT coupling interface

An efficient way to fully couple C-CWatM and (regional) climate models is to use an established coupling software that handles the synchronized data exchange and regridding of the coupling fields. Here, we implement the Ocean–Atmosphere–Sea–Ice–Soil Model Coupling Toolkit, version 5 (OASIS3-MCT, Craig et al., 2017), which is widely adopted in the climate modeling community and thus facilitates interoperability with a wide range of models. It also provides a Python interface (`pyOASIS`), which is essential for integration with C-CWatM, and supports efficient execution of parallelized climate model code. Another advantage of OASIS3-MCT is its non-intrusive syntax, requiring only minimal code modifications within the coupled models, with configuration handled externally via the `namcouple` file.

The technical implementation of OASIS3-MCT within existing models has been described in detail by Masson et al. (2025) and Ho-Hagemann et al. (2024). Therefore, we provide only a brief summary of the key aspects of the coupling interface here, with additional details available in Appendix A. To keep changes in the C-CWatM code minimal, all functions related to the coupling interface are organized within a single file (`pyoasis_cpl.py`). The `initial()` function handles initialization and setup, while the `dynamic()` function manages data exchange by sending and receiving information. Both functions are only called conditionally, based on a newly introduced coupling flag defined in the settings file.

Additionally, we created a simple Python script that serves two main purposes: 1) it acts as a dummy model to test the data exchange via the coupling interface, and 2) it can be used to handle reading and regridding of forcing data. All related functions are organized within the `coupling.py` module, which needs to be adapted for each new forcing dataset. The script reads the model settings, loads the input data, and sends them to C-CWatM using the OASIS3-MCT coupling interface. In this study, we tested the interface using daily model output from the regional climate model REgional MOdel (REMO, Jacob and Podzun, 1997; Pietikäinen et al., 2025) in Europe (see Sect. 5.2 for details). In our tests, reading and regridding the REMO forcing data through the OASIS interface increased the model run time by about 50 %. However, this approach eliminates the preprocessing step previously required for regridding.

The coupling fields to be exchanged are specified in the `namcouple` configuration file for OASIS3-MCT, where time transformations and regridding methods are also defined. Here, we use conservative remapping for runoff and groundwater recharge and a simple distance weighting for soil water content and evaporation over water.

4.2 Optional model calibration

The decision to calibrate a hydrological model largely depends on its intended application. When accurate hydrological predictions are required - such as for decisions on water resource management or climate impact assessments - calibration can

https://doi.org/10.5194/egusphere-2026-2366
Preprint. Discussion started: 13 May 2026

improve model performance and alignment with observed data. However, calibration also introduces notable limitations. Model results become highly sensitive to the spatial distribution of observational data, often leading to overfitting in data-rich basins and unreliable results in data-sparse regions. This is particularly concerning, as these underrepresented areas are often the most vulnerable to water-related challenges. Calibration can also mask underlying uncertainties of model parameterizations, as well as potential errors and/or biases in the underlying input data.

Despite these concerns, we provide an optional calibration framework for C-CWatM and advise users to carefully evaluate whether calibration aligns with their specific modeling objectives. Like in CWatM, the calibration routine is built on the DEAP Python framework (Fortin et al., 2012), which uses the NSGA-II algorithm (Deb et al., 2002) for single objective optimization. The objective function used is the modified version of the Kling-Gupta efficiency (KGE) (Kling et al., 2012), which quantifies the agreement between observed and simulated river discharge by balanced assessment of correlation, bias and variability.

Calibration can be performed at global, regional, or catchment scales. A list of recommended calibration parameters is provided in in Tab. 1. Compared to CWatM, C-CWatM includes fewer land surface processes, and therefore we keep only 6 of the 12 calibration parameters originally suggested for CWatM. We extended the list by the 'alpha depletion' variable, which defines the upper soil moisture threshold up to which farmers irrigate. This variable is likely of importance for studies focused on irrigation and could also be set to a fixed value based on a priori knowledge.

In this study, we demonstrate the calibration of C-CWatM for a European domain using 40 gauging stations and 10-year calibration and validation periods. A regionalized approach was applied, that estimates calibration parameters at catchment scale, allowing the derivtion of appropriate parameter sets for both gauged and ungauged catchments. The applied regionalization approach is similar to that proposed by Beck et al. (2016), which estimates calibration parameters based on physio-climatic similarity between a given hydrological catchment and all gauged upstream basins. Further details on station selection, calibration procedures, and regionalization are provided in Appendix C.

4.3 Bias correction

Bias correction is often used in climate and impact modelling to adjust systematic errors in climate model outputs by considering observations or observation-based data. Hydrological models are particularly sensitive to forcing biases, as errors in water-cycle quantities (such as precipitation and evapotranspiration) can propagate within the model, leading to unrealistic estimates of streamflow, soil moisture, and water management. Impact studies, therefore, usually apply bias correction of the forcing data. It is implemented as post-processing of the forcing data using various methods, most commonly quantile mapping. Quantile mapping corrects the statistical distributions of modelled forcing variables based on observed values prior to implementing hydrological simulations.

However, such post-processing of climate model data is not feasible in online-coupled model runs, in which C-CWatM exchanges information at runtime. To address this limitation, C-CWatM provides an optional on-the-fly bias correction. Instead of performing full statistical bias correction dynamically (which would require access to long-term time series at runtime), C-CWatM enables users to provide an a-priori csv-file containing pre-computed, domain-wide quantile correction weights corresponding to those used in quantile mapping. C-CWatM applies these quantile-based adjustment factors to the incoming

https://doi.org/10.5194/egusphere-2026-2366
Preprint. Discussion started: 13 May 2026

Table 1. Optional C-CWatM calibration parameters.

Module	Variable description	Variable name Default value [Range]
Soil	**Infiltration capacity parameter**: empirical shape parameter b of the ARNO model	`arnoBeta_add`: 0.39 [0.01, 1.2]
Routing	**Channel Manning's n factor**: roughness factor in channel routing	`manningsN`: 1.86 [0.1, 10]
Groundwater	**Recession coefficient factor**: factor to adjust the base flow recession constant (the contribution from groundwater to baseflow)	`recessionCoeff_factor`: 5.278 [0.1, 10.0]
Reservoirs and lakes	**Normal storage limit**: the fraction of storage capacity used as normal storage limit	`normalStorageLimit`: 0.44 [0.15, 0.85]
	Lake "A" factor: factor to channel width and weir coefficient as a part of the Poleni's weir equation	`lakeAFactor`: 0.33 [0.33, 3.0]
	Lake and river evaporation factor: adjust open water evaporation	`lakeEvaFactor`: 1.52 [0.5, 3.0]
Water demand	**Alpha depletion for irrigation**: farmers irrigate only up to a fraction of field capacity	`alphaDepl`: 0.7 [0.5, 1.0]

runoff data before internal processing at each time step. This approach enables a computationally efficient distribution-based correction during online coupling and can significantly reduce runoff biases that potentially compromise hydrological performance. While this on-the-fly correction method is simplified, it provides a robust approach to enhance hydrological consistency in coupled climate-water resource simulations. In principle, bias correction could also be applied to soil moisture and other land surface variables. However, the hydrological impact is significantly larger for runoff. Large-scale observational data on land surface variables, such as runoff and soil moisture, are often limited. Due to difficulties obtaining consistent, high-resolution runoff observations, we estimated correction weights from reference CWatM runoff rather than using observational datasets.

4.4 Reduced forcing requirements

C-CWatM requires the following land surface input: runoff, (rootzone) soil moisture, evaporation from open water sources, and drainage/groundwater recharge. However, drainage and evaporation over water surfaces might not be featured in specific land surface and climate models and are often not among the standard output in reanalyses or coordinated modelling experiments (e.g., CMIP, CORDEX). Therefore, C-CWatM provides options to reduce the amount of required forcing data to simplify the coupling process, or to enable fast offline simulations and allow direct use of readily available CORDEX and CMIP6 outputs to generate river discharge and water-management indicators.

If estimates of evaporation over open water surfaces are not available, C-CWatM can estimate this quantity using either net radiation (Milly and Dunne, 2016) or surface air temperature (Hamon, 1961) as proxies. Details about these methods are provided in the user guide (C-CWatM user guide, 2026). Additionally, if drainage data is not available, C-CWatM allows scaling groundwater recharge based on runoff using an optional scaling factor. However, because the relationship between these

https://doi.org/10.5194/egusphere-2026-2366
Preprint. Discussion started: 13 May 2026

parameters is not well defined and typically nonlinear, this approach provides only a rough first-order estimate of groundwater recharge. Therefore, it is not recommended to conduct an explicit analysis of groundwater quantities in that case.

5 Data

5.1 Input maps

Like CWatM, C-CWatM can be run at both global and regional scales. Regional domains can be either specified by a set of coordinates or by a mask map. The boundary conditions of C-CWatM are defined by various global datasets. Generally, we use the same input datasets as CWatM (Burek et al., 2020) provided at two resolutions of 0.5° and 0.5′, excluding those related to soil processes and surface fluxes, which correspond to model components that have been removed. An overview can be found in Tab. B1 in the Appendix. The datasets include data on land cover fractions, groundwater, a lake and reservoir database, and a flow direction map. Multiple socioeconomic datasets are used to estimate water demand of the domestic, industrial, and livestock sectors.

Irrigation requires data on irrigated areas, crop coefficients, and soil moisture thresholds - specifically field capacity and wilting point. In CWatM, the latter two are calculated internally using soil parameters from the HSWD database (FAO, 2012), applying a combination of van Genuchten's soil water retention model (Van Genuchten, 1980) and Mualem's hydraulic conductivity model (Mualem, 1976). In C-CWatM, we revised this approach so that field capacity and wilting point can now be provided as external datasets. This allows for better consistency with coupled climate models, which may use different soil parameterizations. For offline simulations, we supply precomputed datasets using the same method as in CWatM, based on HSWD parameters and the Mualem- and van Genuchten model.

5.2 Forcing data

To test the default forcing using the four standard forcing variables, we use model output from the REMO2020 regional climate model (Pietikäinen et al., 2025). The simulations were performed over the EURO-CORDEX domain on a rotated grid with 0.11° resolution, corresponding to approximately 12.5×12.5 km, which is only slightly coarser than the 5′ resolution of C-CWatM. The model setup includes 27 vertical levels and uses ERA5 as boundary conditions, with a time step of 1 h. The simulation was initialized in 1979, and for this study we use data until the year 2019. For C-CWatM forcing (Fig. 2), we use daily aggregated values of the variables runoff (`RUNOFF`), drainage (`DRAIN`) and evaporation over water surfaces (`EVAPW`). Soil moisture in REMO is calculated using a bucket scheme with a single soil layer extending to the root depth. The absolute water content in this layer (`WS` in m) is converted to relative soil saturation (in `%`) by dividing by the soil water holding capacity.

To evaluate C-CWatM using reduced forcing, we consider a simplified set of hydrometeorological variables: runoff (`mrro`), total soil moisture (`mrso`), and near-surface air temperature (`tas`). These variables are obtained from 13 EURO-CORDEX simulations (Jacob et al., 2020) conducted at a resolution of 0.11° covering the period from 1960 to 2005. We selected all

https://doi.org/10.5194/egusphere-2026-2366
Preprint. Discussion started: 13 May 2026

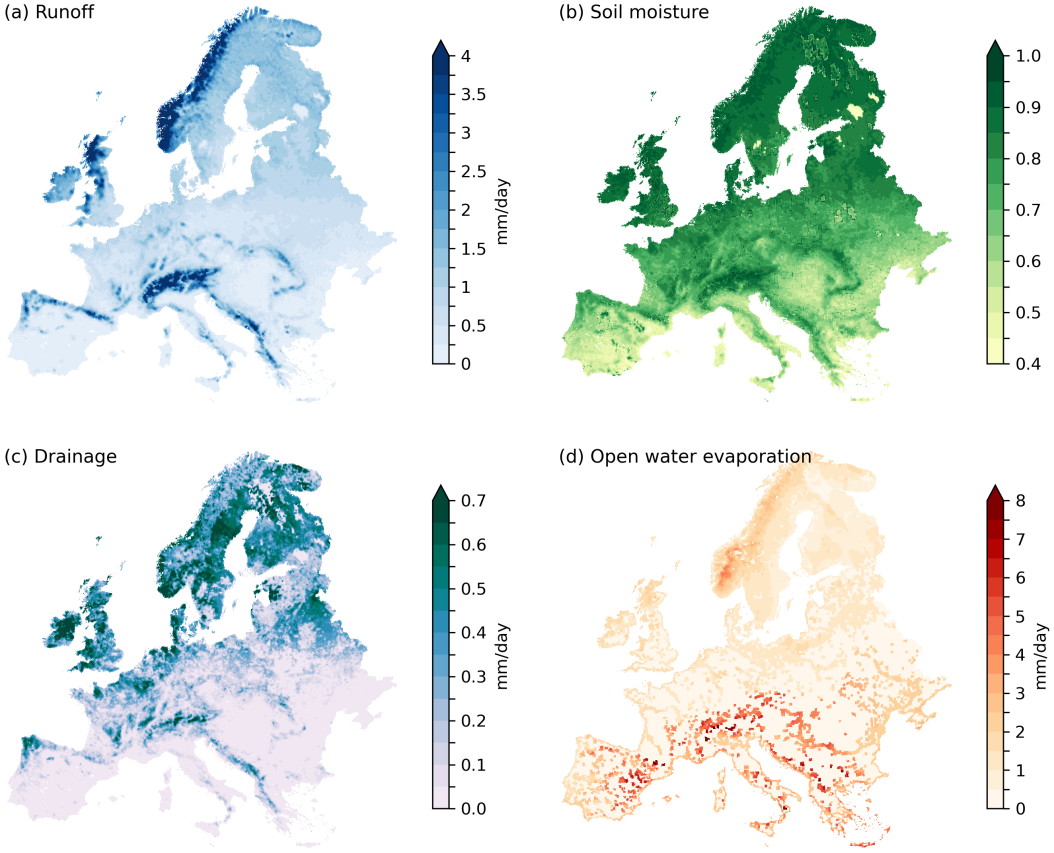

Figure 2. Multi-year averages between 1990 and 2019 of C-CWatM forcing derived from REMO2020 output for (a) runoff, (b) soil moisture, (c) drainage, and (d) open water evaporation.

simulations that provide runoff, temperature and soil moisture as output variables, namely from the three regional climate models COSMO-CLM, RACMO and REMO, forced by 6 different global climate model simulations (for details see Tab. D1).

The reduced-forcing data enables rapid offline simulations and the direct application of readily accessible CORDEX outputs to calculate river discharge and water management indicators. Since C-CWatM relies on relative soil saturation rather than absolute soil moisture, and since field capacity required for conversion was not consistently available across the models, we implemented a percentile-based normalisation approach to estimate relative soil saturation as $\mathrm{SM}_{relsat} = \mathrm{SM}/\mathrm{SM}_{Q99}$, with SM denoting absolute soil moisture and SM_{Q99} the 99th percentile of absolute soil moisture. This method enables us to convert the variable mrso into relative saturation for each model.

https://doi.org/10.5194/egusphere-2026-2366
Preprint. Discussion started: 13 May 2026

5.3 CWatM model run for comparison

To evaluate spatial patterns in simulated discharge, we consider a reference CWatM simulation (Burek et al., 2020) implemented over the same European domain using a calibrated, regionalised parameter set (see Appendix C). The reference simulation is driven by MSWX meteorological forcing (Beck et al., 2022), which provides globally consistent, observation-based estimates of precipitation, temperature, and other meteorological quantities at high spatio-temporal resolution. The reference CWatM simulation provides a benchmark for evaluating the C-CWatM experiments, enabling us to assess how C-CWatM replicates hydrological dynamics and discharge volumes compared to a sophisticated hydrological simulation. In addition, we use runoff obtained from the CWatM reference run to bias-correct REMO runoff via quantile mapping, providing bias-corrected input for C-CWatM..

6 Test application

To verify and evaluate the performance of C-CWatM, we implemented a set of offline simulations across those major European river basins located entirely within the EURO-CORDEX domain. We used REMO output from 1979 to 2019, remapped to the native 5-minute resolution of C-CWatM using bilinear remapping methods from CDO (Climate Data Operators, Schulzweida, 2023). The first 10 years of forcing data were used to initialise the hydrological simulations, resulting in a 30-year output dataset from 1990 to 2019.

6.1 River discharge and water demand

Using raw climate model output as input without calibrating C-CWatM (default version), the model is able to reproduce European river discharge patterns (see Fig. 3a). The model effectively captures the highest discharge values in the largest rivers across Europe (e.g., Danube, Rhine, Dnieper) and reflects the expected discharge gradients from Northern to Southern Europe and from Alpine to lowland regions. The model simulates water demand from different sectors (see Fig. 3b-e). Domestic water demand is highest in major metropolitan areas in Western and Central Europe (e.g., London, Paris, Randstad, Rhein-Ruhr), aligning with population density. Industrial water demand peaks in highly industrialised areas in the UK, Central Europe, Northern Italy, and Southeastern Europe. Irrigation water demand is highest in irrigated farmlands across Spain, Northern Italy, and Southeastern Europe. Please note that irrigation water demand is generally overestimated in C-CWatM offline simulations, because soil moisture is prescribed as a forcing variable and irrigation is not dynamically coupled within the forcing model. Due to the lack of reliable and spatially consistent reference datasets, evaluating water demand estimates across different sectors at the European level is not feasible within the scope of this study. We focus our evaluation efforts on hydrological performance, for which established observational datasets are available. However, we acknowledge that thoroughly validating water-use estimates remains an important task for future research.

https://doi.org/10.5194/egusphere-2026-2366
Preprint. Discussion started: 13 May 2026

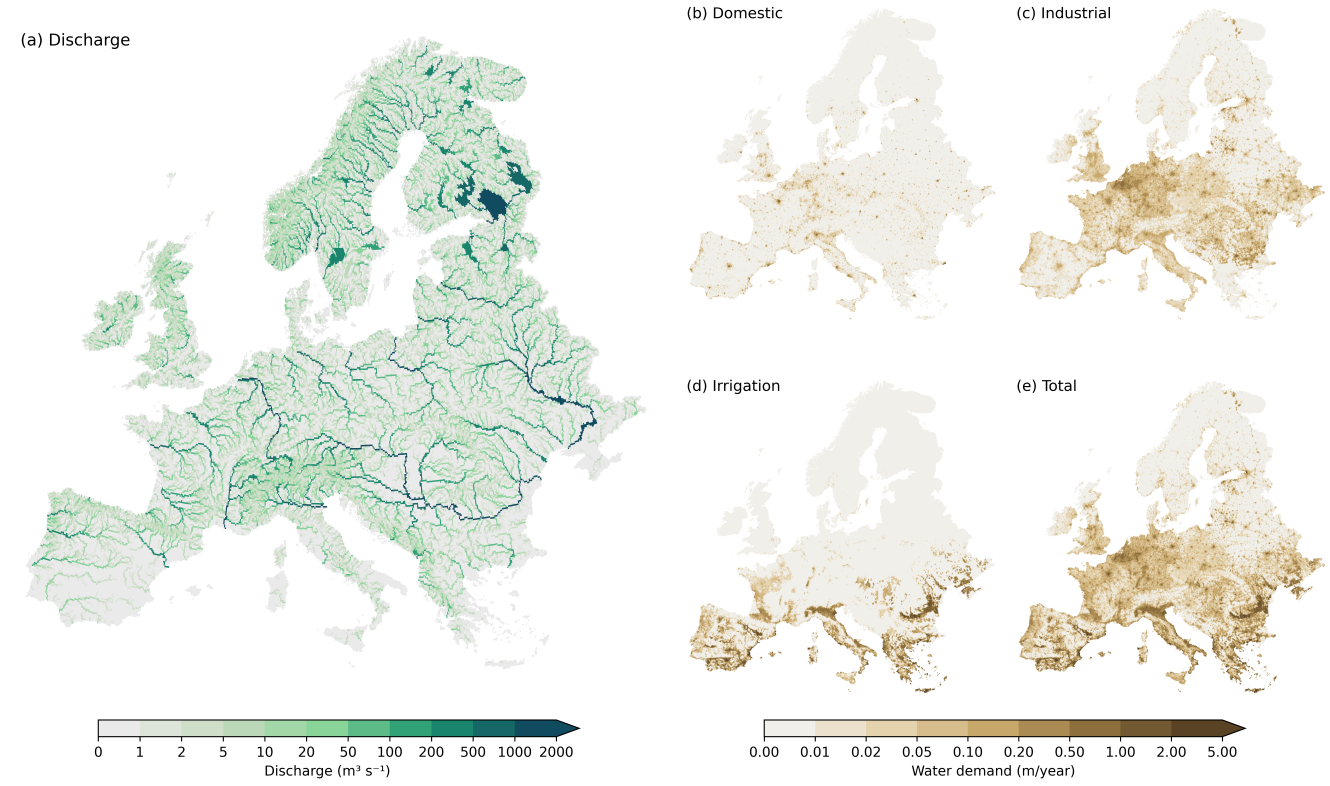

Figure 3. Example output of C-CWatM using raw climate model output without calibration as forcing. Multi-year average (a) discharge and (b) domestic, (c) industrial, (d) irrigation, and (e) total water demand between 1990 and 2019.

6.2 Model validation

To systematically assess the performance of C-CWatM and to better understand the impact of no calibration vs. calibration (noC/C) in combination with no bias correction vs. bias correction (noBC/BC), we implement four distinct model simulations: (noC-noBC): an uncalibrated model simulation (using the C-CWatM default parameter set) forced by raw REMO output, (C-noBC): a calibrated model run considering a regionalised parameter set obtained through calibration using raw REMO output, (noC-BC): an uncalibrated model simulation considering bias-corrected REMO runoff (corrected against CWatM reference runoff), and (C-BC): a calibrated model run considering a regionalised parameter set obtained through calibration using bias-corrected REMO runoff. Comparing results from the four different model simulations enables simultaneous evaluation of model skill, calibration performance, and forcing uncertainties. The noC-noBC simulation provides an estimate of the baseline performance of the C-CWatM model without parameter tuning, highlighting the potential impact of raw climate model biases on hydrological performance. The C-noBC simulation isolates the added value of calibration, allowing for the evaluation of regional calibration using raw climate model output and assessing whether systematic forcing biases can be mitigated through calibration. The noC-BC simulation isolates the added value of bias correction, enabling us to assess whether improving the

https://doi.org/10.5194/egusphere-2026-2366
Preprint. Discussion started: 13 May 2026

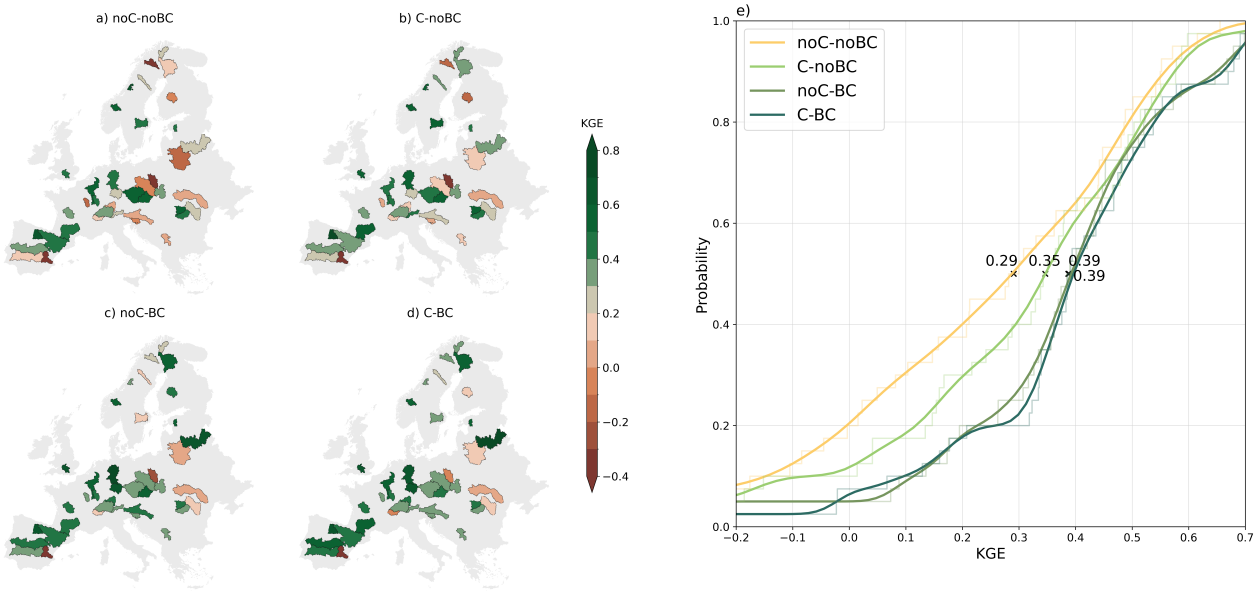

Figure 4. Validation of C-CWatM model simulations (1999-2008) against observed discharge from 40 gauging stations. KGE values are shown for each basin under four scenarios. (a) noC-noBC: no calibration and no bias-correction, (b) C-noBC: calibration and no bias-correction, (c) noC-BC: no calibration and bias-correction, and (d) C-BC: calibration and bias-correction. (e) Empirical cumulative distribution function (pale-colored steplike lines) and the corresponding kernel density estimate (thick lines) of KGE values across all simulations, with median KGE values highlighted.

climate forcing alone increases model performance. The C-BC simulation quantifies the combined effects of bias correction and calibration, helping to determine whether applying calibration under improved forcing conditions results in more robust hydrological simulations and more reliable parameter estimates.

6.2.1 Validation against observed discharge

We consider discharge observations from 40 gauging stations that represent mid-sized river basins across Europe. These stations were used for calibration over 10 years from 1989 to 1998 (see Section 4.2 and Appendix C). For validation, we consider data from 1999 to 2008 and estimate Kling-Gupta Efficiency (KGE) values by comparing observed discharge with simulated discharge from the four model experiments (see Fig. 4). The default noC-noBC simulation already shows reasonable performance, with a median KGE of 0.28 and more than 32 basins with KGE values greater than 0 (see Fig. 4e). Lower KGE values are particularly found in Southern Spain and eastern Europe (see Fig. 4a). When assessing calibration-based simulations without bias correction (C-noBC), overall performance improves with a median KGE of 0.35 and only 4 catchments with KGE values less than 0 (see Fig. 4e). KGE values improve across Europe, with some Eastern European catchments now showing

https://doi.org/10.5194/egusphere-2026-2366
Preprint. Discussion started: 13 May 2026

reasonable performance between 0.2 and 0.4 (see Fig. 4b). Using bias-corrected runoff without calibration (noC-BC) results in a slight increase in the median KGE to 0.38. However, it significantly reduces the number of catchments with very low KGE values (Fig. 4e). Only two catchments remain with a KGE of less than 0, while more than 32 catchments now have a KGE greater than 0.2 (compared to only 27 catchments under C-noBC). Performance improves across all of Europe, with only one poorly performing catchment remaining in Spain and only a few in Eastern Europe (Fig. 4c). When both calibration and bias correction are applied (C-BC), overall performance increases slightly (median KGE at 0.39), such that 20 catchments across Europe now show KGE values greater than 0.4 (see 4d,e).

Systematic discharge biases, resulting from forcing biases, may have a disproportionate impact on low and high flow conditions. We assess percentage biases between observed discharge at 40 gauging stations and simulated discharge from the four model experiments at the 5th quantile (low flow), median level, and 95th quantile (high flow; Fig. 5).

The default noC-noBC simulation suggests an overall increase in discharge variability compared to observed discharge conditions, characterised by lower low flows and higher high flows. Q05 differences indicate an average underestimation of low flows by about 50 % with the largest differences across Southern and Central Europe. In contrast, high flows at Q95 are slightly overestimated (about 20 % on average), with the strongest positive biases in Northern and Eastern Europe, while Spain shows negative biases. Median flow conditions at Q50 display generally small biases, but with a North-South gradient across Europe: positive biases in Northern Europe and negative biases in Southern Europe.

When assessing calibration-based simulations without bias correction (C-noBC), biases are slightly reduced in comparison to noC-noBC, though the spatial distribution of biases across Europe remains similar. However, considering bias-corrected runoff without (noC-BC) and with calibration (C-BC) reveals different spatial patterns and overall negative biases across all quantiles. Overall, while substantial biases are observed across all simulations, many catchments, particularly in Central Europe, remain within a range of moderate biases for median and high flow conditions. Calibration (considering C-noBC and C-BC) generally reduces absolute biases for all considered quantiles. Bias correction against CWatM reference runoff (noC-BC and C-BC) tends to shift biases predominantly towards negative values. At Q5, however, the combination of bias correction and calibration results in the lowest absolute bias values.

6.2.2 Validation against reference simulations

To better understand spatial and mean biases, we assess percentage biases between the simulated discharge from a reference CWatM simulation (see Sect. 5.3) and the simulated discharge from the four model experiments (Fig. 6). The default noC-noBC simulation and the calibration-based simulation without bias correction (C-noBC) show very similar spatial bias patterns (Fig. 6a,b). Positive biases are predominantly found in Northern and Eastern Europe, as well as in many high-altitude regions, such as the Alps, Pyrenees, and Massif Central. Lowland areas in Central and Western Europe are subject to only minor biases, with a slight tendency towards negative values. More substantial negative biases are primarily concentrated along the coasts of Western Europe, particularly in the northwestern regions of the Iberian Peninsula, as well as in parts of Northern Italy and the Balkans. Discharge biases follow inherent biases in REMO runoff (Fig. 7a). Overall, both model runs demonstrate systematic positive biases, affecting both smaller streams, characterised by low discharge values, and larger rivers. The mean percentage

https://doi.org/10.5194/egusphere-2026-2366
Preprint. Discussion started: 13 May 2026

Figure 5. Percentage bias at low (Q05, upper row), median (Q50, middle row), and high (Q95, bottom row) flow levels of C-CWatM model simulations from 1999 to 2008 compared to observed discharges from 40 gauging stations. Percentage biases are shown for each basin under four scenarios. (1st column) noC-noBC: no calibration and no bias-correction, (2nd column) C-noBC: calibration and no bias-correction, (3rd column) noC-BC: no calibration and bias-correction, and (4th column) C-BC: calibration and bias-correction.

https://doi.org/10.5194/egusphere-2026-2366
Preprint. Discussion started: 13 May 2026

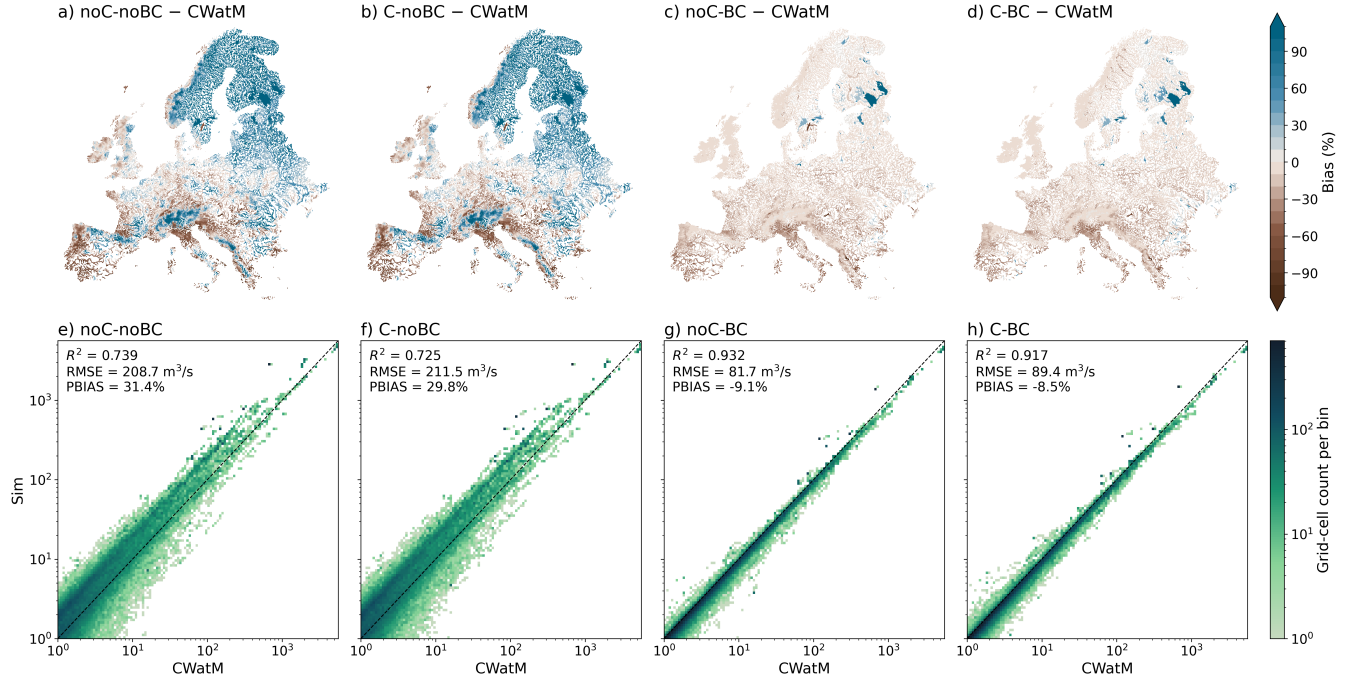

Figure 6. Spatial and pointwise evaluation of mean simulated discharge from 1990 to 2019 under four scenarios relative to the CWatM reference simulation. (a-d): Spatial maps show the percentage bias between 30-yr average discharge for each setup and CWatM under four scenarios: (1st column) noC-noBC, (2nd column) C-noBC, (3rd column) noC-BC, and (4th column) C-BC. (e-h): Density scatter plots comparing grid-cell mean discharge of each setup against CWatM on logarithmic axes. Colours represent the two-dimensional histogram density (grid-cell count per bin). The dashed identity line indicates perfect agreement (black, dashed line). Annotated metrics in each panel provide the explained variance (R^2), root-mean-square error (RMSE), and percentage bias (PBIAS).

bias across all of Europe is 31.4% for the noC-noBC model and 29.8% for the C-noBC model. The root-mean-square errors are considerable, approximately $210 m^3/s$ in both experiments. However, the explained variances are relatively high (larger than 0.7 for both experiments), indicating that, despite the large positive biases, there is generally a good agreement between simulated and reference discharge values. Considering bias-corrected runoff without calibration (noC-BC) and with calibration (C-BC) shows a significant reduction in biases (see Fig. 6c,d). This reduction is expected as runoff from the reference simulation was used for bias correction. Across Europe, biases remain slightly negative, especially in parts of Southern Europe, corresponding to negative biases in bias-corrected runoff (Fig. 7b). However, it highlights how biases in the forcing data can propagate into discharge estimates and underscores the importance of bias correction over calibration for accurately modelling mean discharge values. This is further emphasised when compared to bias-corrected and calibrated simulations (C-BC), which show only a slight improvement in mean percentage bias (-9.1% to -8.5%) but no improvement in RMSE and R^2 when compared to noC-BC simulations.

https://doi.org/10.5194/egusphere-2026-2366
Preprint. Discussion started: 13 May 2026

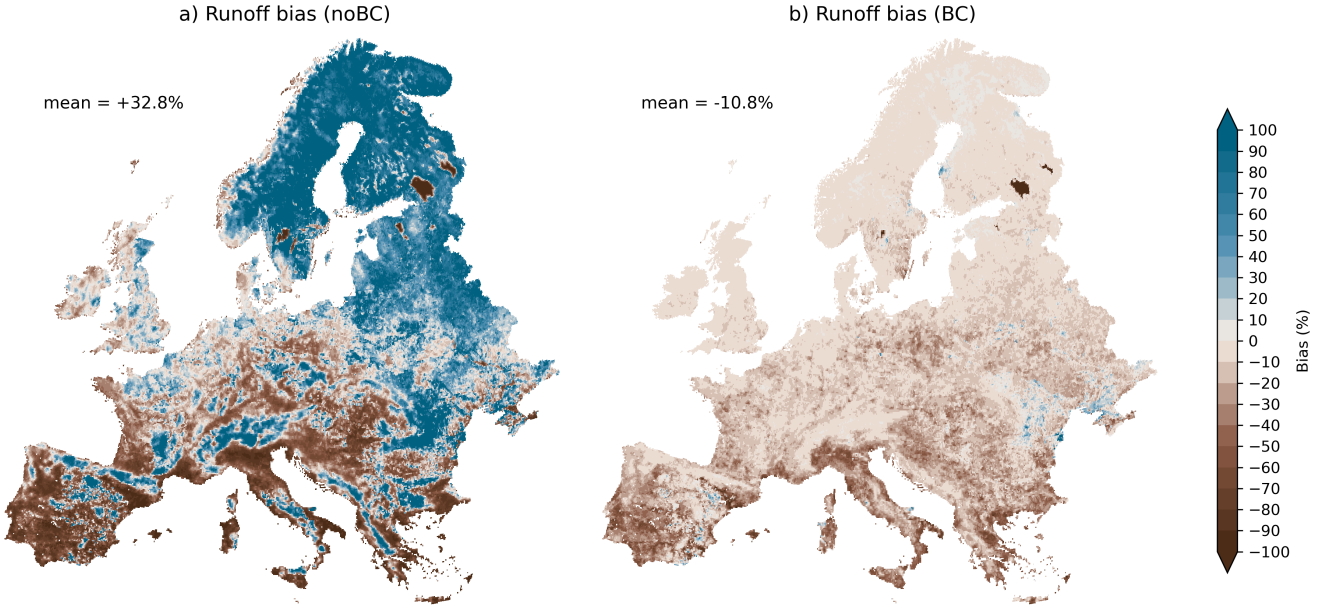

Figure 7. Percentage difference between 30-yr average (1990 to 2019) REMO runoff and CWatM reference runoff (a) before bias correction, and (b) after bias correction.

6.3 Reduced forcing considering EURO-CORDEX simulations

C-CWatM provides the option to use reduced-forcing data to enable fast offline simulations using readily available CORDEX outputs (see Sect. 4.4). We utilise 13 EURO-CORDEX models (see Appendix D) to drive long-term simulations between 1960 to 2005 using a non-bias corrected and non-calibrated version of C-CWatM. We compute mean discharge values for each model and the multi-model average within the overlapping period from 1990 to 2005 and evaluate their performance relative to the CWatM reference simulation (Fig. 8). The forcing from each model shows explained variance values of at least 0.7, with 8 out of the 13 models exceeding 0.9. This indicates strong agreement between the simulated and reference mean discharge values. The lowest explained variances (ranging from 0.7 to 0.8) were associated with the simulations driven by REMO2015 and REMO2009, while the other regional climate models demonstrated higher explained variances above 0.9. Three forcing models have RMSE values above $200 m^3/s$ (highest: $244.7 m^3/s$, MPI-ESM-LR_RACMO22E) and two models below $120 m^3/s$ (lowest: $100.2 m^3/s$, EC-EARTH_CCLM4-8-17). All models showed positive percentage biases, with three models showing biases smaller than 20% (lowest: 14.7%, EC-EARTH_CCLM4-8-17) and 5 models showing significant biases larger than 50% (highest: 74.7%, MPI-ESM-LR_RACMO22E). Despite the presence of systematic biases and residual errors, the overall performance is reasonable, given that each model simulation was implemented without bias correction and without calibration. The multi-model mean supports this conclusion, showing an explained variance of 0.922, an RMSE of $151.5 m^3/s$, and a percentage bias of 40%.

https://doi.org/10.5194/egusphere-2026-2366
Preprint. Discussion started: 13 May 2026

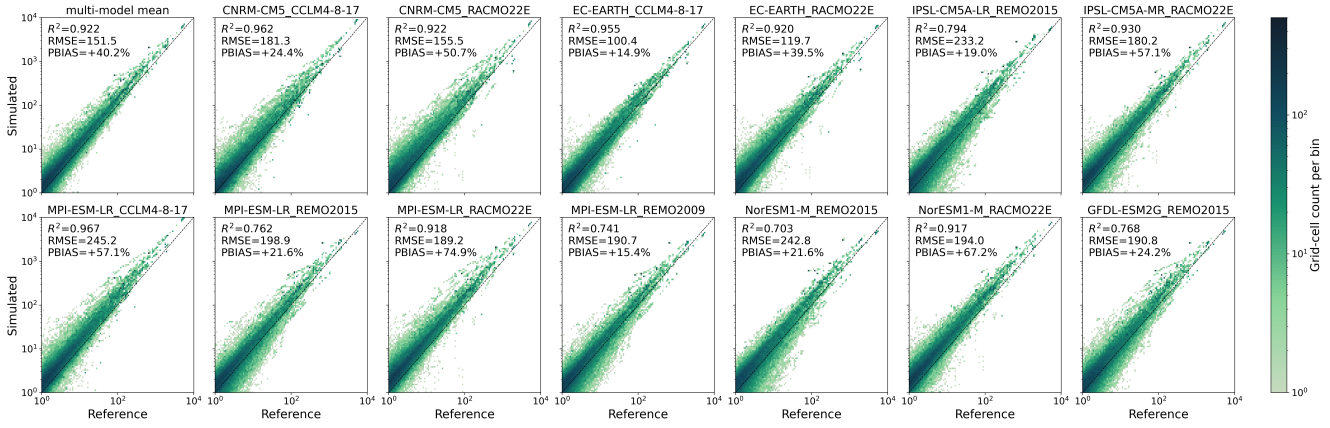

Figure 8. Density scatter plots comparing the mean discharge from 1990 to 2019 of C-CWatM, forced by 13 different EURO-CORDEX model outputs in reduced forcing mode, against a CWatM reference run on logarithmic axes. The multi-model mean is shown in the upper left panel. Colours represent the two-dimensional histogram density (grid-cell count per bin). The dashed identity line indicates perfect agreement (black, dashed line). Annotated metrics in each panel provide the explained variance (R^2), root-mean-square error (RMSE), and percentage bias (PBIAS).

7 Discussion

We have developed C-CWatM, a land-surface-driven version of the large-scale hydrological model CWatM. C-CWatM fills the gap between offline hydrological models and (regional) climate, Earth system, and land surface modelling systems that lack representations of river routing and human water management. Traditional hydrological modelling approaches require atmospheric inputs and are not suitable for two-way coupling with climate and land surface models. In contrast, C-CWatM requires only land-surface input, features a modular structure, and includes a coupling interface for easy integration with climate and land-surface models.

By conducting a series of simulations using raw output from the regional climate model REMO, we found promising skill across a set of 40 medium-sized gauged catchments throughout Europe, even in uncalibrated conditions and without applying any bias correction to the runoff input. This indicates that raw land-surface data from climate models, despite potentially containing systematic errors in their hydroclimatological and land-surface outputs that likely propagate from precipitation biases (Maraun, 2012; Vautard et al., 2021), still enable reasonable estimates of river discharge across many European basins. However, significant discrepancies in modelled discharge remain in various regions, particularly in parts of the Iberian Peninsula and Eastern Europe. Improving model performance can be achieved through calibration and bias correction. While calibration alone results in a modest improvement in model performance against observed discharge, it cannot completely offset the biases in runoff forcing. In contrast, bias correction significantly improves model performance. Using both methods together enables a slight additional increase in performance, particularly in low-flow conditions.

https://doi.org/10.5194/egusphere-2026-2366
Preprint. Discussion started: 13 May 2026

C-CWatM is generally able to translate REMO runoff into realistic hydrological behaviour across Europe, as it closely replicates discharge patterns relative to the reference CWatM simulation. However, systematic spatial biases remain when no calibration and bias correction are considered, due to systematic errors that propagate from the REMO forcing. Positive biases in mean discharge are generally found in northern, eastern, and mountainous regions, while negative biases are located in parts of western and southern Europe. Calibration alone cannot eliminate these patterns, indicating that systematic errors in the input data dominate model performance rather than model parameter optimisation. Bias-correcting runoff significantly reduces spatial biases, highlighting the importance of addressing biases in input data. However, we acknowledge that targeted water management assessments may require further improvement in model performance, while C-CWatM output serves as a baseline estimate. Remaining differences can be largely attributed to input land-surface biases, rather than the routing or water management representations within C-CWatM. Hence, potential biases in runoff forcing remain a significant limitation in coupled modelling systems where sophisticated bias correction is not feasible. C-CWatM, therefore, offers a simple and computationally-efficient on-the-fly bias-correction method during online coupling, which can improve hydrological consistency.

C-CWatM can be implemented using the OASIS coupling interface, which enables online coupling consistent with the practice of linking components of Earth system models. OASIS provides options for regridding and flexible exchange frequencies, and it is compatible with a wide range of existing climate and Earth system models (such as CESM, REMO, WRF, ICON-CLM, and EC-Earth). By coupling with C-CWatM, these models could effectively and routinely represent human-water interactions that are currently not well represented, including features such as river dams, reservoirs, and groundwater pumping. As a result, C-CWatM enables a more realistic assessment of irrigation-climate feedbacks in coupled modelling systems and facilitates climate change adaptation studies focused on issues such as water scarcity and hydroclimatological extremes (particularly low flow conditions).

Some components of C-CWatM require further improvement. While a linear groundwater reservoir may be sufficient for a first-order estimate of groundwater availability, it can introduce significant biases in hydrogeologically complex areas and may negatively impact baseflow estimates. Additionally, the representation of paddy irrigation in C-CWatM is idealised compared to CWatM, where the surface is covered by a layer of open water. The simplified representation of paddy irrigation in C-CWatM is adequate for the European domain, while associated uncertainties may be more substantial in areas characterised by widespread rice cultivation, such as South and East Asia. It is also important to emphasise that the quality of the input data is crucial for obtaining reasonable model skill. Although the model structure can compensate for moderate biases in the input data, a thorough assessment of the validity and quality of any input data is essential.

However, the modular structure and extensibility of C-CWatM provide opportunities for improvement and the implementation of new process representations. For instance, these improvements could include a more dynamic irrigation representation based on plant phenology and growth characteristics obtained from the coupled climate and land surface models, as well as more advanced groundwater representations that build on the existing linkage between CWatM and ModFlow (Guillaumot et al., 2022). In fully coupled simulations, it is also crucial to consider surface-atmosphere interactions in areas with managed dams and reservoirs (Vanderkelen et al., 2021). Methodologically, while pyoasis serves as a blueprint for implementing other

https://doi.org/10.5194/egusphere-2026-2366
Preprint. Discussion started: 13 May 2026

couplers, developing a more standardized interface and coupling workflows could further simplify the implementation of online simulations across a wider range of climate, Earth system and land surface models.

8 Conclusions

This study presents the first release of C-CWatM, a simplified version of CWatM that uses land-surface output as input and can be coupled to climate models. C-CWatM provides a flexible, modular, open-source framework for modelling river routing and human water use. The model is designed for both quick offline and online coupled simulations via OASIS3-MCT. Our analysis indicates that C-CWatM can reasonably simulate large-scale discharge patterns across Europe even without calibration. While calibration improves overall performance, bias correcting the REMO runoff input has a larger effect. Additionally, the reduced-forcing mode enables fast simulations with acceptable accuracy. C-CWatM enables a new set of coupled hydroclimatological experiments, including more realistic representations of irrigation-atmosphere interactions, routine assessments of water scarcity dynamics in historical and future climate simulations, and evaluations of the hydroclimatological impacts of reservoirs and dams.

C-CWatM adds an important new layer to existing modelling systems by consistently representing water management processes, enabling coordinated multi-model assessments in which hydrology, land-surface processes and atmospheric dynamics are evaluated within a single coupled framework. Estimates of water availability and irrigation demand can be linked directly and dynamically to changing climate conditions rather than relying on prescribed conditions. Coupled simulations that utilise the C-CWatM framework can provide substantial support to water managers by providing integrated estimates of water availability, irrigation demand, and scarcity risks driven by changing hydroclimatic conditions. Results from a coupled modelling system, therefore, enable more comprehensive planning of irrigation strategies, municipal water management, hydropower, and dam/reservoir releases under both current and future climate scenarios, particularly in regions facing current and future water challenges.

Code availability. C-CWatM Version 1.0 is permanently archived on Zenodo at https://doi.org/10.5281/zenodo.19709771 (Greve et al., 2026b). Additionally, C-CWatM is openly available under a GNU General Public License v3.0 on GitHub (https://github.com/UWaRes/c-cwatm, last access: 24 April 2026), including a detailed user guide and example settings files. The parent model CWatM is available on GitHub (https://github.com/iiasa/CWatM, last access: 24 April 2026). The calibration routine is permanently archived on Zenodo at https://doi.org/10.5281/zenodo.19709251 (Schmitt et al., 2026) and available on GitHub (https://github.com/UWaRes/c-cwatm_calibration, last access: 24 April 2026). Data analysis was performed using Python 3.11.4. We used JupyterHub (https://jupyter.org/hub, last access: 24 April 2026) within the JupyterHub @ DKRZ environment (https://jupyterhub.dkrz.de, last access: 24 April 2026) provided by the German Climate Computing Centre (DKRZ, https://www.dkrz.de, last access: 24 April 2026). Python scripts and Jupyter notebooks for the analysis are available on Zenodo at https://doi.org/10.5281/zenodo.19724767 (Greve et al., 2026a).

https://doi.org/10.5194/egusphere-2026-2366
Preprint. Discussion started: 13 May 2026

Data availability. Input maps can be obtained through CWatM repositories (0.5°: https://github.com/iiasa/CWatM-Earth-30min, last access: 24 April 2026; 5′: https://drive.google.com/drive/folders/1HqcBj5fD6DHJpOe-t_6JHFMKFtubghZf, last access: 24 April 2026). C-CWatM-specific soil input maps are featured in the permanently archived version on Zenodo at https://doi.org/10.5281/zenodo.19709771 (Greve et al., 2026b) and available in the C-CWatM GitHub repository (https://github.com/UWaRes/c-cwatm, last access: 24 April 2026). C-CWatM model output is available on Zenodo at https://doi.org/10.5281/zenodo.19708464 (Greve and Schmitt, 2026b). REMO forcing data used in this study is available on Zenodo (runoff: https://doi.org/10.5281/zenodo.19681407 (Greve and Schmitt, 2026c), soil moisture, drainage and evaporation over water: https://doi.org/10.5281/zenodo.19708470 (Greve and Schmitt, 2026a)). EURO-CORDEX data (Jacob et al., 2020) is available at https://esgf-metagrid.cloud.dkrz.de/ (last access: 24 April 2026). Calibration parameter maps are available from the C-CWatM calibration repository permanently archived on Zenodo at https://doi.org/10.5281/zenodo.19709251 (Schmitt et al., 2026) and on GitHub (https://github.com/UWaRes/c-cwatm_calibration, last access: 24 April 2026)

https://doi.org/10.5194/egusphere-2026-2366
Preprint. Discussion started: 13 May 2026

Appendix A: Structure of the OASIS3-MCT coupling interface

All details about how to run the coupled model (on levante) and how to adjust the code for different forcing datasets are described in the C-CWatM user guide (C-CWatM user guide, 2026). An example of the namcouple file can be found on GitHub (https://github.com/UWaRes/c-cwatm, last access: 24 April 2026)

A1 Implementation of the coupling interface in C-CWatM

Building on CWatM's general model structure, all functionalities related to the OASIS3-MCT coupler are grouped in the file `management_modules/pyoasis_cpl.py`, which contains the `pyoasis_cpl()` class, as well as additional coupling functions. Like all other processes in C-CWatM, `pyoasis_cpl()` consists of the methods `initial()`, which is called in `cwatm_inital.py`, and `dynamic()`, which is called in `cwatm_dynamic.py`. The coupling routine is only called when the newly introduced flag `coupl_flag` in the settings file is set to `'oasis_cpl'`. This structure allows for an implementation with only minimal changes in the main C-CWatM code.

The function `initial()` groups all code required for the initialization of OASIS3-MCT, while `dynamic()` performs the data exchange at specified time steps. During model initialization, the `initial()` method sets up the coupling interface by creating an OASIS component for C-CWatM using `pyoasis.Component()` and defining the local MPI communicator and grid partitioning using `pyoasis.SerialPartition()`. The C-CWatM grid and the corresponding land-sea-mask are written to netCDF files using `pyoasis.Grid()`. The coupling fields, which are the required forcing variables runoff, groundwater recharge, soil moisture, and evaporation over water, are defined using `pyoasis.Var()`. The names of the coupling variables defined here have to match the declarations in the `namcouple` file.

The `dynamic()` method manages the exchange of data between the different OASIS model components. At each exchange interval – defined in the `namcouple` configuration file – C-CWatM receives the variables specified in the initial phase using the pyOASIS `get()` method. If the units of the received variables differ from those expected by C-CWatM, conversion factors are applied. These factors can be defined in the settings file under `[METEO]` using the format `conv_<varname>`. After applying the C-CWatM land mask, the received fields are assigned to the corresponding internal C-CWatM variables: runoff (`runoff`), groundwater recharge (`sum_gwRecharge`), soil moisture (`rootzoneSM`), and evaporation over water (`EWRef`). If C-CWatM should be configured to send fields to the second model coupled to C-CWatM (e.g. the amount of irrigation water), this would also be implemented in the `dynamic()` method using the pyOASIS `put()` function. Note that any additional variables intended for exchange must be declared and initialized in the `initial()` method and in the `namcouple` file.

A2 Using the OASIS interface to read forcing data

To test the coupling interface, we developed a simple secondary Python script that functions as a dummy model. This script reads forcing data from input files and sends the fields to C-CWatM via OASIS3-MCT. Beyond testing purposes, the script is also useful for handling forcing data that have not yet been regridded to the C-CWatM grid. Since OASIS automatically

https://doi.org/10.5194/egusphere-2026-2366
Preprint. Discussion started: 13 May 2026

performs the regridding, no manual preprocessing is required before initiating the model run. For each new forcing dataset, a dedicated dummy script is required, typically named in the format `run_oasis_forcing_<dataset>.py`. In this study, we tested the coupling interface with output from the REgional climate MOdel (REMO). All additional functions used by the dummy script are aggregated in the file `management_modules/coupling.py`. This file should be extended or modified whenever additional types of forcing data need to be incorporated into the workflow. The type of forcing data is specified using a newly introduced model flag (e.g. `'remo'`) in the `[COUPLING]` section of the settings file.

The dummy model is structured as follows: model run specifications are loaded using the functions `parse_settings_file()` and `read_modelrun_info()`. The function `read_remo_info()` is responsible for retrieving details about the forcing data, including grid coordinates and other relevant metadata. Similar to C-CWatM, the dummy model is initialized as a component within the OASIS3-MCT coupling framework, and its grid specifications are written to file using the function `init_oasis_forcing()`. The class `MeteoForc2Var` manages all functionalities related to reading the forcing data at each time step. Dataset-specific aspects – such as file naming conventions (`get_filename()`) and variable names (`varnames_dict()`) – are handled separately to ensure flexibility and compatibility with different data sources. During the time loop, the respective forcing data are loaded and subsequently sent to C-CWatM via OASIS3-MCT. If the forcing dataset provides soil moisture for multiple layers, the function `interp_rootzoneSM_2d` can be used to calculate the root zone soil moisture.

A3 The namcouple configuration file

The `namcouple` file contains all configuration settings for the OASIS coupler (see Valcke et al. (2021) for details). Each coupling field to be exchanged is described in a dedicated section, specifying the variable names, the coupling frequency, and the source and target grids. If time transformations (e.g. averaging or maximum value), pre- or post-processing steps, or spatial interpolations are required, they are also configured here. In this study, we use the `SCRIPR` routines for regridding. The interpolation weights are computed during the model's initial run and saved to file, which accelerates subsequent interpolations.

To ensure accurate water mass conservation, we use a conservative regridding method (`CONSERV`) for runoff and groundwater recharge. For variables that do not require conservation – such as soil water content (expressed as a percentage) and potential evaporation over water (a surface flux) – we apply a distance-weighted interpolation method (`DISTWGT`). In the `namcouple` file, the two different regridding methods are defined by the following lines:

```
1: DISTWGT LR SCALAR LATLON 1 4
```

for distance-weighted nearest-neighbor interpolation considering the 4 closest neighbors, and

```
1: CONSERV LR SCALAR LATLON 1 FRACAREA FIRST
```

for first-order conservative remapping with normalization based on the source cell intersected areas (`FRACAREA`). The normalization requires the corner locations for each grid cell, which can be computed using the functions provided within

https://doi.org/10.5194/egusphere-2026-2366
Preprint. Discussion started: 13 May 2026

`management_modules/grid_tools.py`. The additional keywords state that we use logically rectangular grids, scalar fields, and a latitude-longitude-based bin search with 1 bin.

Appendix B: Overview of input data

C-CWatM standard input data are the same as for CWatM and available at resolutions of 0.5° (https://github.com/iiasa/CWatM-Earth-30min, last access: 24,04.2026) and 0.5′ (https://drive.google.com/drive/folders/1HqcBj5fD6DHJpOe-t_6JHFMKFtubghZf, last access: 24.04.2026).

Table B1. C-CWatM input maps. Adapted from Burek et al. (2020), their Tab. 1.

Dataset	**Source**	**Original spatial resolution**	**Submodule in C-CWatM**
Elevation	SRTM (Jarvis et al., 2008); Hydro1k (USGS, 2002)	3′, 1 km	Water demand
Flow direction map	DDM30 (Döll and Lehner, 2002); DRT (Wu et al., 2011)	30′ and 5′	Routing, lakes
Lakes and reservoirs	HydroLakes database (Messager et al., 2016; Lehner et al., 2011)	Shapefile	Lakes, routing
Groundwater	GLHYMPS (Huscroft et al., 2018)	–	Groundwater
Land cover	Landcover fraction derived for CWatM (Burek et al., 2020) Irrigated areas (Döll and Siebert, 2002; Siebert et al., 2005, 2010)	5′ 5′	Land cover Water demand
Crop coefficient	MIRCA2000 (Portmann et al., 2010)	5′	Irrigation
Population and GDP	Hyde 3.2 database (Klein Goldewijk et al., 2017) SSP Database at IIASA (Riahi et al., 2017) SSP population and GDP projections: Spatial disaggregation on 30” and 5′ (Jones and O’Neill, 2016; Gao, 2017; Kummu et al., 2018; Gidden et al., 2018)	5′ Country 7.5′, 0.5′	Water demand
Livestock water demand	Gridded livestock densities (FAO, 2007; Steinfeld et al., 2006) Livestock per country (FAO et al., 2012)	5′ Country	Water demand
Industrial water demand	Gridded industrial water data (Shiklomanov, 2000a)	5′	Water demand
Domestic water demand	Domestic water withdrawal per capita (FAO et al., 2012; Gleick et al., 2009)	5′	Water demand

Appendix C: Details of regionalized calibration

In this study, we calibrated (and validated) C-CWatM using daily discharge data from the Global Runoff Data Centre (GRDC) (Global Runoff Data Centre, 2025). Forty stations were selected to represent diverse European conditions, ensuring broad spatial coverage and variation in basin size, climate, hydrology and landscape characteristics. The selected stations report a

https://doi.org/10.5194/egusphere-2026-2366
Preprint. Discussion started: 13 May 2026

mean annual discharge of 15 to 1,000 m^3/s with upstream basin sizes between 5,000 and 100,000 km^2. Data must be available for the period 1989–2008, with less than 5 % missing values in each sub-period 1989–1998 and 1999–2008. All calibration stations are listed in Tab. C1.

C-CWatM model simulations cover the period 1979-2008, starting with two 5-year phases for initialization and spin-up, followed by a 10-year calibration period (1989-1998) and a 10-year validation period (1999-2008). Like in CWatM, the Distributed Evolutionary Algorithms in Python (DEAP) framework (Fortin et al., 2012) is used to set up the calibration routine. We used an initial population size of 100 and a recombination pool size of 16 with 40 generations, which was sufficient to achieve convergence.

In the first calibration step, we derive parameter sets individually optimized for each gauged calibration station's upstream basin. In the next calibration step, we apply a catchment-based regionalization approach similar to that proposed by Beck et al. (2016), which assigns parameters based on physio-climatic similarity. The catchments are delineated according to the level 5 (sub-)basin polygons from HydroBASINS (Lehner and Grill, 2013). Here, we assign new parameter sets for all catchments based on physio-climate similarity between the catchment and all gauged upstream basins, by averaging the parameter sets from the three most similar gauged upstream basins. Dissimilarity is calculated based on three climatic and physiographic characteristics that were identified as strong predictors for average streamflow (Beck et al., 2015): mean annual precipitation, aridity index and surface slope. The two climatic characteristics (mean annual precipitation and aridity index) are both averaged over the period 1990-2019. Mean annual precipitation is calculated directly from MSWX (Beck et al., 2022), the CWatM reference simulation forcing. The aridity index (AI) is defined as the ratio of precipitation (P) to potential evapotranspiration (PET). PET is obtained from a CWatM reference simulation forced with MSWX data and computed within CWatM using FAO Penman-Monteith method (Allen et al., 1998). Surface slope, as the only physiographic characteristic, is provided in the standard CWatM input maps.

Table C1: List of GRDC gauging stations used for validation and calibration

Station number	Station Name	River	Country	Latitude	Longitude
6113050	Almourol	Tagus River	Portugal	39.4610	-8.3750
6116200	Pulo do Lobo	Rio Guadiana	Portugal	37.8030	-7.6330
6226800	Tortosa	Rio Ebro	Spain	40.8133	0.5207
6212740	Valladolid-Pisuerga	Rio Pisuerga	Spain	41.6598	-4.7329
6227510	Huerto Mulet	Rio Jucar	Spain	39.1870	-0.4104
6606655	Kingston	River Thames	United Kingdom	51.4154	-0.3077
6421100	Lith	Meuse	Netherlands	51.8200	5.4500
6123400	Nouatre	Vienne	France	47.0488	0.5444
6125100	Mas-d'Agenais	Rio Garona	France	44.3889	0.3011
6136145	Uckange	Moselle River	France	49.3167	6.1727
6122260	Pont-sur-Seine	Seine	France	48.5238	3.5947

https://doi.org/10.5194/egusphere-2026-2366
Preprint. Discussion started: 13 May 2026

Station number	Station Name	River	Country	Latitude	Longitude
6357500	Eisenhuettenstadt	Oder River	Germany	52.1530	14.6880
6337200	Intschede	Weser	Germany	52.9640	9.1250
6335240	Kleinheubach	Main	Germany	49.7165	9.2246
6342501	Dillingen	Danube River	Germany	48.5684	10.5005
6935051	Basel, Rheinhall	Rhine River	Switzerland	47.5594	7.6167
6939050	Chancy, Aux Ripes	Rhone	Switzerland	46.1530	5.9707
6730501	Polmak Nye	Deatnu	Norway	70.0703	28.0162
6729450	Losna	Losna	Norway	61.3334	10.2775
6731555	Bertnem	Namsen	Norway	64.4681	12.0587
6233410	Oevre Stockholm	Norrstrom	Sweden	59.3000	18.0700
6233510	Granaker	Vindelalven	Sweden	64.2233	19.7036
6232911	Pajala Pumphus	Tornealven	Sweden	67.2074	23.3959
6854700	Isohaara	Kemijoki	Finland	65.7833	24.5500
6854250	Leppavesi, Luusua	Kymijoki	Finland	62.2450	25.8879
6172050	Oore	Parnu Jogi	Estonia	58.4631	24.7675
6373304	Jekabpils	Daugava	Latvia	56.4976	25.8915
6574150	Smalininkai	Nemunas	Lithuania	55.0756	22.5797
6458450	Szczucin	Vistula	Poland	50.3269	21.0772
6457870	Nowa Wies Podgorna	Warta	Poland	52.1417	17.5900
6140400	Decin	Elbe River	Czech Republic	50.7822	14.2096
6142150	Moravsky Jan	Morava	Slovakia	48.6021	16.9358
6243050	Kirchbichl - Bichlwang	Inn	Austria	47.5233	12.0939
6444600	Csenger	Somes	Hungary	47.8322	22.7030
6545050	Catez I	Sava	Slovenia	45.8932	15.6097
6646800	Donji Miholjac C.S.	Drava River	Croatia	45.7746	18.1724
6547110	Jasika	Juzna Morava	Serbia	43.6083	21.2952
6742700	Lungoci	Siret	Romania	45.5559	27.5122
6744201	Alba Iulia	Maros	Romania	46.0375	23.5817
6781800	Tighina (Bendery)	Dniester	Moldova, Republic of	46.8306	29.4711

Appendix D: EURO-CORDEX ensemble

We use 13 EURO-CORDEX simulations (Jacob et al., 2020) implemented at a resolution of 0.11° that provide runoff, temperature and soil moisture as output variables (see Table D1). We consider EURO-CORDEX data covering the period from 1950

https://doi.org/10.5194/egusphere-2026-2366
Preprint. Discussion started: 13 May 2026

to 2005 to force C-CWatM in reduced forcing mode. The period from 1950 to 1959 was used for spin-up, and output data are available from 1960 to 2005. The forcing data was regridded to the C-CWatM 5′ grid using bilinear remapping.

Table D1. Combinations of regional climate models (RCMs) and global climate models (GCMs) providing the required forcing data (runoff, total soil moisture, and near-surface air temperature).

RCM / GCM	CNRM-CM5	EC-EARTH	IPSL-CM5A	MPI-ESM-LR	NorESM-1M	GFDL-ESM2G
CCLM4-8-17	X	X		X		
RACMO22E	X	X	X	X	X	
REMO2015			X	X	X	X
REMO2009				X		

https://doi.org/10.5194/egusphere-2026-2366
Preprint. Discussion started: 13 May 2026

Author contributions. PG conceptualised the model, led the model development, implemented the model experiments, performed the analysis and wrote parts of the manuscript. AUS contributed to the code, implemented the coupling and calibration routine, wrote the User Guide and parts of the manuscript. SJS and AC performed model calibration and contributed to code development, methodology writing, and reviewing. PB contributed to conceptualisation, methodology writing, and reviewing.

Competing interests. All authors declare no competing interests

Acknowledgements. This research was carried out in the UWaRes project supported by the Helmholtz Association Initiative and Networking Fund. This work used resources of the Deutsches Klimarechenzentrum (DKRZ, https://www.dkrz.de) granted by its Scientific Steering Committee (WLA) under project ID ch0636. The authors thank Pia Freisen for providing an internal review of the manuscript.

https://doi.org/10.5194/egusphere-2026-2366
Preprint. Discussion started: 13 May 2026

References

Allen, R. G., Pereira, L. S., Raes, D., Smith, M., et al.: FAO Irrigation and drainage paper No. 56, Rome: food and agriculture organization of the United Nations, 56, e156, 1998.

Alter, R. E., Im, E.-S., and Eltahir, E. A. B.: Rainfall consistently enhanced around the Gezira Scheme in East Africa due to irrigation, Nat. Geosci., 8, 763–767, 2015.

Arboleda-Obando, P. F., Ducharne, A., Yin, Z., and Ciais, P.: Validation of a new global irrigation scheme in the land surface model ORCHIDEE v2.2, Geoscientific Model Development, 17, 2141–2164, https://doi.org/10.5194/gmd-17-2141-2024, 2024.

Asmus, C., Hoffmann, P., Pietikäinen, J.-P., Böhner, J., and Rechid, D.: Modeling and evaluating the effects of irrigation on land–atmosphere interaction in southwestern Europe with the regional climate model REMO2020–iMOVE using a newly developed parameterization, Geoscientific Model Development, 16, 7311–7337, https://doi.org/10.5194/gmd-16-7311-2023, 2023.

Beck, H. E., De Roo, A., and van Dijk, A. I.: Global maps of streamflow characteristics based on observations from several thousand catchments, Journal of Hydrometeorology, 16, 1478–1501, https://doi.org/10.1175/JHM-D-14-0155.1, 2015.

Beck, H. E., van Dijk, A. I., De Roo, A., Miralles, D. G., McVicar, T. R., Schellekens, J., and Bruijnzeel, L. A.: Global-scale regionalization of hydrologic model parameters, Water Resources Research, 52, 3599–3622, https://doi.org/10.1002/2015WR018247, 2016.

Beck, H. E., Van Dijk, A. I., Larraondo, P. R., McVicar, T. R., Pan, M., Dutra, E., and Miralles, D. G.: MSWX: Global 3-hourly 0.1 bias-corrected meteorological data including near-real-time updates and forecast ensembles, Bulletin of the American Meteorological Society, 103, E710–E732, https://doi.org/10.1175/BAMS-D-21-0145.1, 2022.

Burek, P., Satoh, Y., Kahil, T., Tang, T., Greve, P., Smilovic, M., Guillaumot, L., Zhao, F., and Wada, Y.: Development of the Community Water Model (CWatM v1.04) – a high-resolution hydrological model for global and regional assessment of integrated water resources management, Geoscientific Model Development, 13, 3267–3298, https://doi.org/10.5194/gmd-13-3267-2020, 2020.

Burek, P. A., van der Knijff, J., and de Roo, A.: LISFLOOD-distributed water balance and flood simulation model-revised user manual 2013, Publications Office of the European Union, https://doi.org/10.2788/24719, 2013.

C-CWatM user guide: Schmitt, A. and Greve, P., Zenodo, https://doi.org/10.5281/zenodo.19709582, 2026.

Chow, V., Maidment, D., and Mays, L.: Applied Hydrology; McGrawHill: New York, NY, USA, 1998.

Craig, A., Valcke, S., and Coquart, L.: Development and performance of a new version of the OASIS coupler, OASIS3-MCT_3.0, Geoscientific Model Development, 10, 3297–3308, https://doi.org/10.5194/gmd-10-3297-2017, 2017.

De Roo, A., Wesseling, C., and Van Deursen, W.: Physically based river basin modelling within a GIS: the LISFLOOD model, Hydrological Processes, 14, 1981–1992, https://doi.org/10.1002/1099-1085(20000815/30)14:11/12<1981::AID-HYP49>3.0.CO;2-F, 2000.

Deb, K., Pratap, A., Agarwal, S., and Meyarivan, T.: A fast and elitist multiobjective genetic algorithm: NSGA-II, IEEE Transactions on Evolutionary Computation, 6, 182–197, https://doi.org/10.1109/4235.996017, 2002.

Decharme, B., Costantini, M., and Colin, J.: A Simple Approach to Represent Irrigation Water Withdrawals in Earth System Models, Journal of Advances in Modeling Earth Systems, 17, e2024MS004 508, https://doi.org/https://doi.org/10.1029/2024MS004508, 2025.

D'Odorico, P., Davis, K. F., Rosa, L., Carr, J. A., Chiarelli, D., Dell'Angelo, J., Gephart, J., MacDonald, G. K., Seekell, D. A., Suweis, S., and Rulli, M. C.: The global food-energy-water nexus, Rev. Geophys., 56, 456–531, 2018.

Döll, P. and Lehner, B.: Validation of a new global 30-min drainage direction map, Journal of Hydrology, 258, 214–231, https://doi.org/10.1016/S0022-1694(01)00565-0, 2002.

https://doi.org/10.5194/egusphere-2026-2366
Preprint. Discussion started: 13 May 2026

Döll, P. and Siebert, S.: Global modeling of irrigation water requirements, Water Resources Research, 38, 8–1–8–10, https://doi.org/10.1029/2001WR000355, 2002.

Druel, A., Munier, S., Mucia, A., Albergel, C., and Calvet, J.-C.: Implementation of a new crop phenology and irrigation scheme in the ISBA land surface model using SURFEX_v8.1, Geoscientific Model Development, 15, 8453–8471, https://doi.org/10.5194/gmd-15-8453-2022, 2022.

Elliott, J., Deryng, D., Müller, C., Frieler, K., Konzmann, M., Gerten, D., Glotter, M., Flörke, M., Wada, Y., Best, N., Eisner, S., Fekete, B. M., Folberth, C., Foster, I., Gosling, S. N., Haddeland, I., Khabarov, N., Ludwig, F., Masaki, Y., Olin, S., Rosenzweig, C., Ruane, A. C., Satoh, Y., Schmid, E., Stacke, T., Tang, Q., and Wisser, D.: Constraints and potentials of future irrigation water availability on agricultural production under climate change, Proc. Natl. Acad. Sci. U. S. A., 111, 3239–3244, 2014.

FAO: Gridded livestock of the world, Food and Agriculture Organization of the United Nations, Rome, p. 131 pp., 2007.

FAO: FAOSTAT online database, available at: http://www.fao.org/faostat (last access: 17 September 2025), 2012.

FAO, IIASA, ISRIC, ISSCAS, and JRC: Harmonized World Soil Database (version 1.2), available at https://www.fao.org/soils-portal/data-hub/soil-maps-and-databases/harmonized-world-soil-database-v12/en/ (last access: 6 October 2025), 2012.

Fortin, F.-A., De Rainville, F.-M., Gardner, M.-A. G., Parizeau, M., and Gagné, C.: DEAP: Evolutionary algorithms made easy, The Journal of Machine Learning Research, 13, 2171–2175, 2012.

Gao, J.: Downscaling Global Spatial Population Projections from 1/8-degree to 1-km Grid Cells, National Center for Atmospheric Research, Boulder, CO, USA, 2017.

Gidden, M. J., Fujimori, S., van den Berg, M., Klein, D., Smith, S. J., van Vuuren, D. P., and Riahi, K.: A methodology and implementation of automated emissions harmonization for use in Integrated Assessment Models, Environmental Modelling and Software, 105, 187–200, https://doi.org/https://doi.org/10.1016/j.envsoft.2018.04.002, 2018.

Gleick, P. H., Cooley, H., Cohen, M. J., Morikawa, M., Morrison, J., and Palaniappan, M.: The world's water 2008-2009: The biennial report on freshwater resources, vol. 6, Island Press, 2009.

Global Runoff Data Centre: Daily discharge data [Dataset], https://grdc.bafg.de/data/data_portal/ (last access: ...), 2025.

Greve, P. and Schmitt, A.: C-CWatM example forcing: REMO soil moisture, drainage and evaporation over water 1979-2019, Europe, 5arcmin, Zenodo [data], https://doi.org/10.5281/zenodo.19708470, 2026a.

Greve, P. and Schmitt, A.: C-CWatM output: REMO forcing, 1990-2019, Europe, 5arcmin, Zenodo [data], https://doi.org/10.5281/zenodo.19708464, 2026b.

Greve, P. and Schmitt, A.: C-CWatM example forcing: REMO runoff 1979-2019, Europe, 5arcmin, Zenodo [data], https://doi.org/10.5281/zenodo.19681407, 2026c.

Greve, P., Kahil, T., Mochizuki, J., Schinko, T., Satoh, Y., Burek, P., Fischer, G., Tramberend, S., Burtscher, R., Langan, S., and Wada, Y.: Global assessment of water challenges under uncertainty in water scarcity projections, Nat. Sustain., 1, 486–494, 2018.

Greve, P., Burek, P., Guillaumot, L., van Meijgaard, E., Aalbers, E., Smilovic, M. M., Sperna-Weiland, F., Kahil, T., and Wada, Y.: Low flow sensitivity to water withdrawals in Central and Southwestern Europe under 2 K global warming, Environ. Res. Lett., 18, 094 020, 2023.

Greve, P., Schmitt, A. U., Miralles, D. G., McDermid, S., Findell, K. L., García-García, A., and Peng, J.: Observational evidence of increased afternoon rainfall downwind of irrigated areas, Nat. Commun., 16, 3415, 2025.

Greve, P., Schmitt, A., and Schreiber, S. J.: C-CWatM Analysis: Jupyter Notebooks and Settings Files, Zenodo [misc], https://doi.org/10.5281/zenodo.19724768, 2026a.

https://doi.org/10.5194/egusphere-2026-2366
Preprint. Discussion started: 13 May 2026

Greve, P., Schmitt, A., Schreiber, S. J., Clédat, A., and Burek, P.: UWaRes/c-cwatm: Initial release of Climate-CWatM, , Zenodo [code], https://doi.org/10.5281/zenodo.19709771, 2026b.

Guillaumot, L., Smilovic, M., Burek, P., de Bruijn, J., Greve, P., Kahil, T., and Wada, Y.: Coupling a large-scale hydrological model (CWatM v1.1) with a high-resolution groundwater flow model (MODFLOW 6) to assess the impact of irrigation at regional scale, Geosci. Model Dev., 15, 7099–7120, 2022.

Haase, P., Bowler, D. E., Baker, N. J., Bonada, N., Domisch, S., Garcia Marquez, J. R., Heino, J., Hering, D., Jähnig, S. C., Schmidt-Kloiber, A., Stubbington, R., Altermatt, F., Álvarez-Cabria, M., Amatulli, G., Angeler, D. G., Archambaud-Suard, G., Jorrín, I. A., Aspin, T., Azpiroz, I., Bañares, I., Ortiz, J. B., Bodin, C. L., Bonacina, L., Bottarin, R., Cañedo-Argüelles, M., Csabai, Z., Datry, T., de Eyto, E., Dohet, A., Dörflinger, G., Drohan, E., Eikland, K. A., England, J., Eriksen, T. E., Evtimova, V., Feio, M. J., Ferréol, M., Floury, M., Forcellini, M., Forio, M. A. E., Fornaroli, R., Friberg, N., Fruget, J.-F., Georgieva, G., Goethals, P., Graça, M. A. S., Graf, W., House, A., Huttunen, K.-L., Jensen, T. C., Johnson, R. K., Jones, J. I., Kiesel, J., Kuglerová, L., Larrañaga, A., Leitner, P., L'Hoste, L., Lizée, M.-H., Lorenz, A. W., Maire, A., Arnaiz, J. A. M., McKie, B. G., Millán, A., Monteith, D., Muotka, T., Murphy, J. F., Ozolins, D., Paavola, R., Paril, P., Peñas, F. J., Pilotto, F., Polášek, M., Rasmussen, J. J., Rubio, M., Sánchez-Fernández, D., Sandin, L., Schäfer, R. B., Scotti, A., Shen, L. Q., Skuja, A., Stoll, S., Straka, M., Timm, H., Tyufekchieva, V. G., Tziortzis, I., Uzunov, Y., van der Lee, G. H., Vannevel, R., Varadinova, E., Várbíró, G., Velle, G., Verdonschot, P. F. M., Verdonschot, R. C. M., Vidinova, Y., Wiberg-Larsen, P., and Welti, E. A. R.: The recovery of European freshwater biodiversity has come to a halt, Nature, 620, 582–588, 2023.

Hamon, W. R.: Estimating potential evapotranspiration, Journal of the Hydraulics Division, 87, 107–120, https://doi.org/10.1061/JYCEAJ.0000599, 1961.

Hanasaki, N., Yoshikawa, S., Pokhrel, Y., and Kanae, S.: A global hydrological simulation to specify the sources of water used by humans, Hydrol. Earth Syst. Sci., 22, 789–817, 2018.

Ho-Hagemann, H. T. M., Maurer, V., Poll, S., and Fast, I.: Coupling the regional climate model ICON-CLM v2.6.6 to the Earth system model GCOAST-AHOI v2.0 using OASIS3-MCT v4.0, Geoscientific Model Development, 17, 7815–7834, https://doi.org/10.5194/gmd-17-7815-2024, 2024.

Holland, R. A., Scott, K. A., Flörke, M., Brown, G., Ewers, R. M., Farmer, E., Kapos, V., Muggeridge, A., Scharlemann, J. P. W., Taylor, G., Barrett, J., and Eigenbrod, F.: Global impacts of energy demand on the freshwater resources of nations, Proc. Natl. Acad. Sci. U. S. A., 112, E6707–16, 2015.

Huang, Y., Salama, M. S., Krol, M. S., Su, Z., Hoekstra, A. Y., Zeng, Y., and Zhou, Y.: Estimation of human-induced changes in terrestrial water storagethrough integration of GRACE satellite detection and hydrological modeling: A case study of the Yangtze River basin, Water Resour. Res., 51, 8494–8516, 2015.

Huang, Z., Yuan, X., and Liu, X.: The key drivers for the changes in global water scarcity: Water withdrawal versus water availability, J. Hydrol. (Amst.), 601, 126 658, 2021.

Huscroft, J., Gleeson, T., Hartmann, J., and Börker, J.: Compiling and Mapping Global Permeability of the Unconsolidated and Consolidated Earth: GLobal HYdrogeology MaPS 2.0 (GLHYMPS 2.0), Geophysical Research Letters, 45, 1897–1904, https://doi.org/10.1002/2017GL075860, 2018.

Jacob, D. and Podzun, R.: Sensitivity studies with the regional climate model REMO, Meteorol. Atmos. Phys., 63, 119–129, 1997.

Jacob, D., Teichmann, C., Sobolowski, S., Katragkou, E., Anders, I., Belda, M., Benestad, R., Boberg, F., Buonomo, E., Cardoso, R. M., et al.: Regional climate downscaling over Europe: perspectives from the EURO-CORDEX community, Regional environmental change, 20, 51, https://doi.org/10.1007/s10113-020-01606-9, 2020.

https://doi.org/10.5194/egusphere-2026-2366
Preprint. Discussion started: 13 May 2026

Jarvis, A., Reuter, H. I., Nelson, A., and Guevara, E.: Hole-filled SRTM for the globe Version 4, available from the CGIARCSI SRTM 90m Database http://srtm.csi.cgiar.org (last access: 17 September 2025), 2008.

Jia, H., Qian, H., Zheng, L., Feng, W., Wang, H., and Gao, Y.: Alterations to groundwater chemistry due to modern water transfer for irrigation over decades, Sci. Total Environ., 717, 137 170, 2020.

Jones, B. and O'Neill, B. C.: Spatially explicit global population scenarios consistent with the Shared Socioeconomic Pathways, Environmental Research Letters, 11, 084 003, https://doi.org/10.1088/1748-9326/11/8/084003, 2016.

Klein Goldewijk, K., Beusen, A., Doelman, J., and Stehfest, E.: Anthropogenic land use estimates for the Holocene – HYDE 3.2, Earth System Science Data, 9, 927–953, https://doi.org/10.5194/essd-9-927-2017, 2017.

Kling, H., Fuchs, M., and Paulin, M.: Runoff conditions in the upper Danube basin under an ensemble of climate change scenarios, Journal of Hydrology, 424-425, 264–277, https://doi.org/https://doi.org/10.1016/j.jhydrol.2012.01.011, 2012.

Kummu, M., Taka, M., and Guillaume, J. H.: Gridded global datasets for gross domestic product and human development index over 1990–2015, Scientific data, 5, 1–15, https://doi.org/10.1038/sdata.2018.4, 2018.

Lawston-Parker, P., Santanello, Jr, J. A., and Chaney, N. W.: Investigating the response of land–atmosphere interactions and feedbacks to spatial representation of irrigation in a coupled modeling framework, Hydrol. Earth Syst. Sci., 27, 2787–2805, 2023.

Lehner, B. and Grill, G.: Global river hydrography and network routing: baseline data and new approaches to study the world's large river systems, Hydrological Processes, 27, 2171–2186, https://doi.org/10.1002/hyp.9740, 2013.

Lehner, B., Liermann, C. R., Revenga, C., Vörösmarty, C., Fekete, B., Crouzet, P., Döll, P., Endejan, M., Frenken, K., Magome, J., Nilsson, C., Robertson, J. C., Rödel, R., Sindorf, N., and Wisser, D.: High-resolution mapping of the world's reservoirs and dams for sustainable river-flow management, Frontiers in Ecology and the Environment, 9, 494–502, https://doi.org/10.1890/100125, 2011.

Li, H., Lo, M.-H., Ryu, D., Peel, M., and Zhang, Y.: Possible increase of air temperature by irrigation, Geophys. Res. Lett., 49, 2022.

Li, J., Zhang, S., Obulkasim, O., Lu, X., Wei, Z., Yuan, H., Li, L., Zeng, J., Yang, D., and Dai, Y.: Impact of reservoirs on local precipitation-temperature coupling relationships, Geophys. Res. Lett., 50, 2023.

Lv, M., Ma, Z., and Yuan, N.: Attributing terrestrial water storage variations across China to changes in groundwater and human water use, J. Hydrometeorol., 22, 3–21, 2021.

Maina, F. Z., Rosen, D., Abbaszadeh, P., Yang, C., Kumar, S. V., Rodell, M., and Maxwell, R.: Integrating the Interconnections Between Groundwater and Land Surface Processes Through the Coupled NASA Land Information System and ParFlow Environment, Journal of Advances in Modeling Earth Systems, 17, e2024MS004 415, https://doi.org/https://doi.org/10.1029/2024MS004415, 2025.

Maraun, D.: Nonstationarities of regional climate model biases in European seasonal mean temperature and precipitation sums, Geophys. Res. Lett., 39, 2012.

Masson, S., Jullien, S., Maisonnave, E., Gill, D., Samson, G., Le Corre, M., and Renault, L.: An updated non-intrusive, multi-scale, and flexible coupling interface in WRF 4.6.0, Geoscientific Model Development, 18, 1241–1263, https://doi.org/10.5194/gmd-18-1241-2025, 2025.

McDermid, S., Nocco, M., Lawston-Parker, P., Keune, J., Pokhrel, Y., Jain, M., Jägermeyr, J., Brocca, L., Massari, C., Jones, A. D., Vahmani, P., Thiery, W., Yao, Y., Bell, A., Chen, L., Dorigo, W., Hanasaki, N., Jasechko, S., Lo, M.-H., Mahmood, R., Mishra, V., Mueller, N. D., Niyogi, D., Rabin, S. S., Sloat, L., Wada, Y., Zappa, L., Chen, F., Cook, B. I., Kim, H., Lombardozzi, D., Polcher, J., Ryu, D., Santanello, J., Satoh, Y., Seneviratne, S., Singh, D., and Yokohata, T.: Irrigation in the earth system, Nat. Rev. Earth Environ., 4, 435–453, 2023.

Mekonnen, M. M. and Hoekstra, A. Y.: Four billion people facing severe water scarcity, Sci. Adv., 2, e1500 323, 2016.

https://doi.org/10.5194/egusphere-2026-2366
Preprint. Discussion started: 13 May 2026

Messager, M. L., Lehner, B., Grill, G., Nedeva, I., and Schmitt, O.: Estimating the volume and age of water stored in global lakes using a geo-statistical approach, Nature communications, 7, 13 603, https://doi.org/10.1038/ncomms13603, 2016.

Milly, P. C. and Dunne, K. A.: Potential evapotranspiration and continental drying, Nature Climate Change, 6, 946–949, https://doi.org/10.1038/nclimate3046, 2016.

Mishra, V., Ambika, A. K., Asoka, A., Aadhar, S., Buzan, J., Kumar, R., and Huber, M.: Moist heat stress extremes in India enhanced by irrigation, Nat. Geosci., 13, 722–728, 2020.

Mualem, Y.: A new model for predicting the hydraulic conductivity of unsaturated porous media, Water resources research, 12, 513–522, https://doi.org/10.1029/WR012i003p00513, 1976.

Müller Schmied, H., Cáceres, D., Eisner, S., Flörke, M., Herbert, C., Niemann, C., Peiris, T. A., Popat, E., Portmann, F. T., Reinecke, R., Schumacher, M., Shadkam, S., Telteu, C.-E., Trautmann, T., and Döll, P.: The global water resources and use model WaterGAP v2.2d: model description and evaluation, Geosci. Model Dev., 14, 1037–1079, 2021.

Nazemi, A. and Wheater, H. S.: On inclusion of water resource management in Earth system models – Part 1: Problem definition and representation of water demand, Hydrol. Earth Syst. Sci., 19, 33–61, 2015.

Pietikäinen, J.-P., Sieck, K., Buntemeyer, L., Frisius, T., Nam, C., Hoffmann, P., Pop, C., Rechid, D., and Jacob, D.: REMO2020: a modernised modular regional climate model, Geoscientific Model Development, 18, 7907–7949, https://doi.org/10.5194/gmd-18-7907-2025, 2025.

Rappin, E. D., Mahmood, R., Nair, U. S., and Pielke, Sr, R. A.: Land–atmosphere interactions during GRAINEX: Planetary boundary layer evolution in the presence of irrigation, J. Hydrometeorol., 23, 1401–1417, 2022.

Reid, A. J., Carlson, A. K., Creed, I. F., Eliason, E. J., Gell, P. A., Johnson, P. T. J., Kidd, K. A., MacCormack, T. J., Olden, J. D., Ormerod, S. J., Smol, J. P., Taylor, W. W., Tockner, K., Vermaire, J. C., Dudgeon, D., and Cooke, S. J.: Emerging threats and persistent conservation challenges for freshwater biodiversity, Biol. Rev. Camb. Philos. Soc., 94, 849–873, 2019.

Riahi, K., van Vuuren, D. P., Kriegler, E., Edmonds, J., O'Neill, B. C., Fujimori, S., Bauer, N., Calvin, K., Dellink, R., Fricko, O., Lutz, W., Popp, A., Cuaresma, J. C., KC, S., Leimbach, M., Jiang, L., Kram, T., Rao, S., Emmerling, J., Ebi, K., Hasegawa, T., Havlik, P., Humpenöder, F., Da Silva, L. A., Smith, S., Stehfest, E., Bosetti, V., Eom, J., Gernaat, D., Masui, T., Rogelj, J., Strefler, J., Drouet, L., Krey, V., Luderer, G., Harmsen, M., Takahashi, K., Baumstark, L., Doelman, J. C., Kainuma, M., Klimont, Z., Marangoni, G., Lotze-Campen, H., Obersteiner, M., Tabeau, A., and Tavoni, M.: The Shared Socioeconomic Pathways and their energy, land use, and greenhouse gas emissions implications: An overview, Global Environmental Change, 42, 153–168, https://doi.org/10.1016/j.gloenvcha.2016.05.009, 2017.

Rodell, M., Famiglietti, J. S., Wiese, D. N., Reager, J. T., Beaudoing, H. K., Landerer, F. W., and Lo, M.-H.: Emerging trends in global freshwater availability, Nature, 557, 651–659, 2018.

Rosa, L. and Sangiorgio, M.: Global water gaps under future warming levels, Nat. Commun., 16, 1192, 2025.

Schewe, J., Heinke, J., Gerten, D., Haddeland, I., Arnell, N. W., Clark, D. B., Dankers, R., Eisner, S., Fekete, B. M., Colón-González, F. J., Gosling, S. N., Kim, H., Liu, X., Masaki, Y., Portmann, F. T., Satoh, Y., Stacke, T., Tang, Q., Wada, Y., Wisser, D., Albrecht, T., Frieler, K., Piontek, F., Warszawski, L., and Kabat, P.: Multimodel assessment of water scarcity under climate change, Proc. Natl. Acad. Sci. U. S. A., 111, 3245–3250, 2014.

Schmitt, A., Greve, P., Schreiber, S. J., and Clédat, A.: UWaRes/c-cwatm_calibration: Regionalised calibration with 3 physio-climatic parameters, Zenodo [code], https://doi.org/10.5281/zenodo.19709251, 2026.

Schulzweida, U.: CDO User Guide, https://doi.org/10.5281/zenodo.10020800, 2023.

https://doi.org/10.5194/egusphere-2026-2366
Preprint. Discussion started: 13 May 2026

Shiklomanov, I. A.: World water resources and water use: present assessment and outlook for 2025., World Water Scenarios: Analysis (ed.) F.R. Rijsberman, pp. 160-203, London, Earthscan Publ., 2000a.

Shiklomanov, I. A.: Appraisal and Assessment of World Water Resources, Water International, 25, 11–32, https://doi.org/10.1080/02508060008686794, 2000b.

Siebert, S., Döll, P., Hoogeveen, J., Faures, J.-M., Frenken, K., and Feick, S.: Development and validation of the global map of irrigation areas, Hydrology and Earth System Sciences, 9, 535–547, https://doi.org/10.5194/hess-9-535-2005, 2005.

Siebert, S., Burke, J., Faures, J. M., Frenken, K., Hoogeveen, J., Döll, P., and Portmann, F. T.: Groundwater use for irrigation – a global inventory, Hydrology and Earth System Sciences, 14, 1863–1880, https://doi.org/10.5194/hess-14-1863-2010, 2010.

Song, Y., Wei, J., Cheng, H., and Zan, B.: Irrigation in the North China plain regulates the diurnal cycle of precipitation and regional water cycle, Clim. Dyn., 2024.

Steinfeld, H., Gerber, P., Wassenaar, T. D., Castel, V., and De Haan, C.: Livestock's long shadow: environmental issues and options, Food & Agriculture Org., 2006.

Sutanudjaja, E. H., van Beek, R., Wanders, N., Wada, Y., Bosmans, J. H. C., Drost, N., van der Ent, R. J., de Graaf, I. E. M., Hoch, J. M., de Jong, K., Karssenberg, D., López López, P., Peßenteiner, S., Schmitz, O., Straatsma, M. W., Vannametee, E., Wisser, D., and Bierkens, M. F. P.: PCR-GLOBWB 2: a 5 arcmin global hydrological and water resources model, Geosci. Model Dev., 11, 2429–2453, 2018.

Tapiador, F. J. and Navarro, A.: Coupling human dynamics with the physics of climate: a path towards human Earth Systems Models, Environ. Res.: Climate, 2024.

Taranu, S. I., Lawrence, D. M., Wada, Y., Tang, T., Kluzek, E., Rabin, S., Yao, Y., De Hertog, S. J., Vanderkelen, I., and Thiery, W.: Bridging the gap: a new module for human water use in the Community Earth System Model version 2.2. 1, Geoscientific Model Development, 17, 7365–7399, https://doi.org/10.5194/gmd-17-7365-2024, 2024.

Thiery, W., Visser, A. J., Fischer, E. M., Hauser, M., Hirsch, A. L., Lawrence, D. M., Lejeune, Q., Davin, E. L., and Seneviratne, S. I.: Warming of hot extremes alleviated by expanding irrigation, Nat. Commun., 11, 290, 2020.

Udias, A., Gentile, A., Burek, P., De Roo, A., Bouraoui, F., Vandecasteele, I., Lavalle, C., and Bidoglio, G.: Multi-Criteria Framework to Assess Large Scale Water Resources Policy Measures, Water, 8, https://doi.org/10.3390/w8090370, 2016.

USGS: Hydro1K, Land Processes Distributed Active Archive Center (LP DAAC), USGS: Geological Survey Center for Earth Resources Observation and Science, 2002.

Valcke, S., Craig, T., Maisonnave, E., and Coquart, L.: OASIS3MCT User Guide, OASIS3-MCT 5.0, CERFACS, CERFACS TR/CMGC/21/161, 2021.

Valmassoi, A., Dudhia, J., Di Sabatino, S., and Pilla, F.: Evaluation of three new surface irrigation parameterizations in the WRF-ARW v3.8.1 model: the Po Valley (Italy) case study, Geoscientific Model Development, 13, 3179–3201, https://doi.org/10.5194/gmd-13-3179-2020, 2020.

Van Genuchten, M. T.: A closed-form equation for predicting the hydraulic conductivity of unsaturated soils, Soil science society of America journal, 44, 892–898, https://doi.org/10.2136/sssaj1980.03615995004400050002x, 1980.

Vanderkelen, I., van Lipzig, N. P. M., Sacks, W. J., Lawrence, D. M., Clark, M. P., Mizukami, N., Pokhrel, Y., and Thiery, W.: Simulating the Impact of Global Reservoir Expansion on the Present-Day Climate, Journal of Geophysical Research: Atmospheres, 126, e2020JD034 485, https://doi.org/https://doi.org/10.1029/2020JD034485, 2021.

Vautard, R., Kadygrov, N., Iles, C., Boberg, F., Buonomo, E., Bülow, K., Coppola, E., Corre, L., van Meijgaard, E., Nogherotto, R., Sandstad, M., Schwingshackl, C., Somot, S., Aalbers, E., Christensen, O. B., Ciarlo, J. M., Demory, M.-E., Giorgi, F., Jacob, D., Jones, R. G.,

https://doi.org/10.5194/egusphere-2026-2366
Preprint. Discussion started: 13 May 2026

Keuler, K., Kjellström, E., Lenderink, G., Levavasseur, G., Nikulin, G., Sillmann, J., Solidoro, C., Sørland, S. L., Steger, C., Teichmann, C., Warrach-Sagi, K., and Wulfmeyer, V.: Evaluation of the large EURO-CORDEX regional climate model ensemble, J. Geophys. Res Atmos., 126, 2021.

Vörösmarty, C. J. and Sahagian, D.: Anthropogenic disturbance of the terrestrial water cycle, Bioscience, 50, 753, 2000.

Wada, Y., van Beek, L. P. H., and Bierkens, M. F. P.: Modelling global water stress of the recent past: on the relative importance of trends in water demand and climate variability, Hydrology and Earth System Sciences, 15, 3785–3808, https://doi.org/10.5194/hess-15-3785-2011, 2011.

Wu, H., Kimball, J. S., Mantua, N., and Stanford, J.: Automated upscaling of river networks for macroscale hydrological modeling, Water Resources Research, 47, https://doi.org/10.1029/2009WR008871, 2011.

Xu, X., Chen, F., Barlage, M., Gochis, D., Miao, S., and Shen, S.: Lessons Learned From Modeling Irrigation From Field to Regional Scales, Journal of Advances in Modeling Earth Systems, 11, 2428–2448, https://doi.org/https://doi.org/10.1029/2018MS001595, 2019.

Yang, Z., Dominguez, F., Zeng, X., Hu, H., Gupta, H., and Yang, B.: Impact of irrigation over the California Central Valley on regional climate, J. Hydrometeorol., 18, 1341–1357, 2017.

Yao, Y., Vanderkelen, I., Lombardozzi, D., Swenson, S., Lawrence, D., Jägermeyr, J., Grant, L., and Thiery, W.: Implementation and Evaluation of Irrigation Techniques in the Community Land Model, Journal of Advances in Modeling Earth Systems, 14, e2022MS003 074, https://doi.org/10.1029/2022MS003074, 2022.

Yokohata, T., Kinoshita, T., Sakurai, G., Pokhrel, Y., Ito, A., Okada, M., Satoh, Y., Kato, E., Nitta, T., Fujimori, S., Felfelani, F., Masaki, Y., Iizumi, T., Nishimori, M., Hanasaki, N., Takahashi, K., Yamagata, Y., and Emori, S.: MIROC-INTEG-LAND version 1: a global biogeochemical land surface model with human water management, crop growth, and land-use change, Geoscientific Model Development, 13, 4713–4747, https://doi.org/10.5194/gmd-13-4713-2020, 2020.

Yoon, J., Klassert, C., Selby, P., Lachaut, T., Knox, S., Avisse, N., Harou, J., Tilmant, A., Klauer, B., Mustafa, D., Sigel, K., Talozi, S., Gawel, E., Medellín-Azuara, J., Bataineh, B., Zhang, H., and Gorelick, S. M.: A coupled human-natural system analysis of freshwater security under climate and population change, Proc. Natl. Acad. Sci. U. S. A., 118, e2020431 118, 2021.

Zhang, Z., Prein, A. F., He, C., Liu, C., Miguez-Macho, G., Chen, F., Abolafia-Rosenzweig, R., Lin, T.-S., and Rasmussen, R.: Moisture from US Corn Belt fuels more intense convective storms, Commun. Earth Environ., 2025.

Zhou, T., Leung, L. R., Leng, G., Voisin, N., Li, H.-Y., Craig, A. P., Tesfa, T., and Mao, Y.: Global irrigation characteristics and effects simulated by fully coupled land surface, river, and water management models in E3SM, Journal of Advances in Modeling Earth Systems, 12, e2020MS002 069, 2020.